A pseudo-local heat transfer approach in a low tube to particle diameter ratio packed bed catalytic reactor: Oxidative Dehydrogenation of ethane as a case study

A. Romero-Limones[1,2], Jeroen Poissonnier[2], Joris W. Thybaut[2*], Carlos O. Castillo[1*]

[1] Laboratory of Catalytic Reactor Engineering Applied to Chemical and Biological Systems, Universidad Autónoma Metropolitana, Av. San Rafael Atlixco 186, 09340, Mexico City, Mexico.

[2] Laboratory for Chemical Technology, Ghent University, Technologiepark 125, B-9052 Ghent, Belgium

Corresponding authors: Carlos O. Castillo (coca@xanum.uam.mx) and Joris W. Thybaut (joris.thybaut@ugent.be)

Nomenclature

Roman letters

a_s	External surface to particle volume ratio, $m_s^2\ m_r^{-3}$	T_s	Solid temperature, K
C_n	Molar concentration of component n in the fluid phase, kmol m_f^{-3}	T_{ss}	Fluid temperature at steady state, K
$C_{n,s}$	Molar concentration of component n in the solid phase, kmol m_f^{-3}	$T_{w,in}$	Temperature at the internal surface of the tube wall, K
$C_{n,s,ss}$	Molar concentration of component n in the solid phase at steady state, kmol m_f^{-3}	T_δ	Temperature at the internal heat boundary layer surface, K
$C_{n,ss}$	Molar concentration of component n in the fluid phase at steady state, kmol m_f^{-3}	u_z	Superficial velocity, $m_f^3\ m_r^{-2}\ h^{-1}$
Cp_f	Specific heat capacity of the fluid at constant pressure, kJ $kg_f^{-1}\ K^{-1}$	$u_{z,0}$	Superficial velocity at the bed inlet, $m_f^3\ m_r^{-2}\ h^{-1}$
Cp_s	Specific heat capacity of the solid at constant pressure, kJ $kg_s^{-1}\ K^{-1}$	U_w	Global heat transfer coefficient, kJ $m_r^{-2}\ h^{-1}\ K^{-1}$
d_p	Particle diameter, m_s	v_z	Axial component of the interstitial velocity, $m_r\ h^{-1}$
d_t	Tube diameter, m_r	$v_{z,ss}$	Axial component of the interstitial velocity at steady state, $m_r\ h^{-1}$
$\mathbf{D}(\mathbf{r})$	Solid-fluid resistance vector, kg $m_r^{-2}\ s^{-2}$	W_i	weight factor assigned to the i-collocation point
$D(r)_z$	z-component of the solid-fluid resistances vector $\mathbf{D}(\mathbf{r})$, kg $m_r^{-2}\ s^{-2}$	X_n	Conversion of component n, $X_n = \frac{C_{n,0} - C_n}{C_{n,0}}$

$D_{eff,r}$	Radial mass dispersion coefficient, $m_r^2\ h^{-1}$	Y_n	Yield of component n, $Y_n = \frac{C_n - C_{n,0}}{C_{C,0}}$
$D_{eff,z}$	Axial mass dispersion coefficient, $m_r^2\ h^{-1}$	z	Axial position, m_r
g_z	Axial component of gravity, $m_r\ h^{-2}$	**Greek letters**	
G	Superficial mass flow rate, kg $m_r^{-2}\ h^{-1}$	α	Ergun's coefficient related to viscous solid-fluid contributions
h_g	Interfacial heat transfer coefficient, W $m_s^{-2}\ K^{-1}$	β	Ergun's coefficient related to inertial solid-fluid contributions
h_w	Wall heat transfer coefficient, W $m_r^{-2}\ K^{-1}$	$\delta_{HT,in}$	Internal heat boundary layer thickness, m_r
$h_{w,ext}$	External wall heat transfer coefficient, W $m_r^{-2}\ K^{-1}$	$\delta_{HT,ext}$	External heat boundary layer thickness, m_r
$h_{w,in}$	Internal wall heat transfer coefficient, W $m_r^{-2}\ K^{-1}$	ΔH_i	Reaction enthalpy, kJ mol^{-1}
$\underline{\mathbf{H}}$	Apparent permeability tensor, m_r^2	ΔP_z	Axial pressure drop, kg $m_r^{-1}\ h^{-2}$
$H(r)_{zz}$	z-component of the tensor $\underline{\mathbf{H}}$, kg $m_r^{-2}\ s^{-2}$	ε	Void fraction, $m_f^3\ m_r^{-3}$
$k_{1,h}$	Slope parameter of the $k_{eff,r,PL}(r)$	ε_0	Averaged void fraction, $m_f^3\ m_r^{-3}$
$k_{2,h}$	Damping parameter of the $k_{eff,r,PL}(r)$	θ_n	Fractional surface coverage of component n
$k_{eff,r}$	Radial effective thermal conductivity, W $m^{-1}\ K^{-1}$	μ_f	Dynamic viscosity, $kg_f\ m_r^{-1}\ h^{-1}$
$k^0_{eff,r}$	Static contribution of the radial effective conductivity, W $m^{-1}\ K^{-1}$	μ_{eff}	Effective viscosity, $kg_f\ m_r^{-1}\ h^{-1}$

$\langle k_{eff,r} \rangle_{core}$	Averaged radial effective thermal conductivity of the packed bed core zone, W m^{-1} K^{-1}
$k_{eff,r,PLA}(r)$	Pseudo-local radial effective thermal conductivity, W m^{-1} K^{-1}
$k_{eff,z}$	Axial effective thermal conductivity, W m_r^{-1} K^{-1}
k_i	Rate coefficient of reaction i, mmol g_{cat}^{-1} h^{-1}
k_g	Interfacial mass transfer coefficient, m_f^3 m_s^{-2} h^{-1}
K	Packed bed permeability, m_r^2
K_z	Packed bed pseudo-permeability, m_r
K_n	Adsorption equilibrium coefficient for component n, Pa^{-1}
L	Reactor length, m_r
m_j	Partial reaction order of reaction j
p_n	Partial pressure of component n, Pa
p_z	Axial component of pressure, Pa
q_0	Heat flux from the infra-red lamp, W m_r^{-2}
r	Radial position, m_r
r_i	Specific reaction rate of reaction i, mmol g_{cat}^{-1} h^{-1}
R_t	Tube radius, m_r
t	Time, h
T	Fluid temperature, K
T_0	Feed temperature, K
T_b	Salt bath temperature, K
$\nu_{n,i}$	Stoichiometric number of component n in reaction i.
ρ_b	Packed bed density, kg_s m_r^{-3}
ρ_f	Fluid density, kg_f m_f^{-3}
ρ_s	Solid density, kg_s m_s^{-3}

Subscripts

c	Number of carbons
cat	Catalyst
eff	Effective
exp	Experimental
f	Fluid
n	Component n
0	Inlet
p	Particle
r	Reactor
s	Solid
ss	Steady state
t	Tube
$*$	Density of vacant sites

Superscript

0	Static, inlet

Abbreviations:

Acronym

BLA	Boundary Layer Approach	ODH-C_2	Oxidative Dehydrogenation of Ethane
CA	Classical Approach	PF-CBLA	Plug Flow Complete Boundary Layer Approach
CBLA	Complete Boundary Layer Approach	PF-IBLA	Plug Flow Internal Boundary Layer Approach
d_t/d_p	tube to particle diameter ratio	PLA	Pseudo-Local Approach
ER	Eley-Rideal	PL-CBLA	Pseudo-local Complete Boundary Layer Approach
IBLA	Internal Boundary Layer Approach	PL-IBLA	Pseudo-local Internal Boundary Layer Approach
KWT-BC	Know Wall-Temperature Boundary Condition	PL-IHTA	Pseudo-local Internal Heat Transfer Approach
KWT-BLA	Known Wall-Temperature Boundary Layer Approach		

Associated contents:

Supporting information available: Section A presents the details of the KWT-BLA used to compare with the PL-IHT. In Section B, the specifications of the kinetic model used in this work to evaluate the reactor model are described. Section C gives the details of the conventional heat transfer approaches used in literature for the modelling of industrial-scale wall-cooled packed bed reactors. The radial temperature profiles at different axial positions, and the axial temperature profiles for the industrial-scale packed bed following the PL-IHTA and KWT-BLA approaches are illustrated in Section D. Section E presents the assessment of the heat transfer mechanisms in the internal and external heat boundary layer. Lastly, in Section F, the pseudo-local and conventional heat transport approaches are applied to simulate ethane conversion, ethylene selectivity, and net production rate of CO_2 for the oxidative dehydrogenation of ethane in an industrial-scale wall-cooled packed bed reactor.

Abstract

A generalized approach to model heat transfer in an industrial-scale wall-cooled packed bed reactor with a low tube-to-particle diameter ratio (< 8) is proposed and assessed in this work. The modeling approach rests on the realization of experiments carried out in absence of reaction in bench-scale as well as in industrial-scale packed beds. The approximation overcomes historical limitations identified when modeling radial heat transfer mechanisms by applying conventional heat transfer approaches. The methodology leads to the reliable determination of the external wall heat transfer coefficient and pseudo-local radial effective thermal conductivity. The approach allows the quantification of heat transfer resistances through the core, the internal and the external wall of the bed indicating that approximately 30% of the resistances are located along the internal side of the packed bed when it was operated at Particle Reynolds numbers ranging from 700 to 1400. Because of its complex impact on heat transfer, fluid dynamics is accounted for by implementing a methodology that uses pressure drop data and the mass conservation criterion to describe velocity profiles, including the determination of the viscous and inertial resistances caused by solid surfaces at the core and near the wall. Finally, the heat transfer information is transferred to a pseudo-heterogenous model to simulate the performance of an industrial-scale wall-cooled packed bed reactor for the highly exothermic oxidative dehydrogenation of ethane. Simulations demonstrate both the reliability of the proposed heat transfer approach and the limitations of the conventional approximations when describing temperature profiles in a packed bed reactor.

Keywords: Radial heat transfer resistances, external heat transfer resistances, wall-cooled packed-bed reactor, fluid dynamics, pseudo-local effective thermal conductivity.

1. Introduction

Wall-cooled packed bed catalytic reactors with a low tube to particle diameter ratio (d_t/d_p < 8 m_r m_s^{-1}) have been a workhorse in the petrochemical industry for the production of chemical building blocks via the selective oxidation of different hydrocarbons [1–4]. The low d_t/d_p configuration not only reduces the pressure drop compared with those packed beds with high d_t/d_p but provides higher void fraction zones leading to larger interstitial velocities that impact heat and mass transfer mechanisms along the packed bed.

Although this type of reactor has been studied for several decades [5–12], and the low d_t/d_p has favored momentum, heat and mass transport processes, the main challenge that still needs to be addressed is the minimization of the extent of undesired total oxidation reactions. Heat released by these reactions generates hot spots which, in turn, induce catalyst deactivation and selectivity losses. Additionally, because of the presence of total oxidations, the wall-cooled packed bed reactor, is highly sensitive to operating conditions such as the coolant temperature, inlet gas temperature and concentration [1,13,14].

Research efforts, aiming at improving the performance of the wall-cooled packed bed reactor with low d_t/d_p, have been focused on developing pseudo-continuous models to design [1,8,15–21], optimize [22–27] or simply understand the complex interaction between transport phenomena and reaction kinetics in wall-cooled packed bed reactors. Because of its high sensitivity to the operating conditions [1,13,14], a diversity of one [28–30] and two [1,5,8,9,12,13,15,21,31–33] dimensional models, such as pseudo-homogeneous models [1,5,8,9,12,13,15–21,31,33–36], pseudo-heterogeneous models [3,7,16,27,37] or heterogeneous models [38–43], have been assessed. Some models (~5%) have accounted for fluid dynamics [5,33], while others (~ 95%) follow the conventional plug flow approach [1–3,27–29,31,37,44–46]. Today, to the best of our knowledge, there is no pseudo-continuous model that can accurately describe the performance of a wall-cooled packed bed reactor

[3,5,31,33,44,47]. Even when, for some systems, reaction kinetics and fluid dynamics have been accurately assessed [33], heat transfer characterization remains the main bottleneck when modeling selective oxidations [5,33].

Firstly, although fluid dynamics is, nowadays, most often neglected when modeling a wall-cooled packed bed reactor [3,27,31,37,44,46,48], it is well-accepted that it impacts heat transfer mechanisms and, hence, the prediction of the temperature profiles. Navier-Stokes-Darcy-Forchheimer (NSDF) based models [5,36,38,41,42,49] or Brinkman- Darcy-Forchheimer (BDF) based models [15,50,51], including the two-zones-based models [33,52], have been coupled to the heat and mass transfer governing equations to predict the temperature and concentration profiles, respectively, in the wall-cooled packed bed reactor. Nevertheless, most of these models are not conservative [3,5,31], which can be attributed to the methodology implemented to determine transfer parameters such as the effective viscosity (μ_{eff}), which accounts for the effect of solid surfaces on fluid dynamics near the reactor wall, and the parameters α and β, which take the solid-fluid interactions at the core of the reactor into account [53]. Secondly, along with a reliable kinetic description, the appropriate description of temperature profiles in the wall-cooled packed bed reactor depends on the acquisition of reliable heat transfer parameters: the radial effective thermal conductivity ($k_{eff,r}$), internal wall heat transfer coefficient ($h_{w,in}$), external wall heat transfer coefficient ($h_{w,ext}$), and wall heat transfer coefficient (h_w). Although different methodologies have been proposed for their determination for over 70 years, most of them present several limitations:

- The wall heat transfer coefficient, h_w, lumps the internal heat transfer resistances encountered in the internal heat boundary layer, $\delta_{HT,in}$, the wall conductivity, k_w, and the heat transfer resistances encountered in the external heat boundary layer, $\delta_{HT,ext}$ [2,8,19,46,54–58]. Although those mechanisms can be characterized by decoupling the

h_w into a $h_{w,in}$, k_w and $h_{w,ext}$, respectively, the role of each parameter in the region near the wall of the packed bed reactor, i.e., the heat transfer resistances, is not clear [59].

- The parameters h_w and $k_{eff,r}$ are rarely determined while accounting for fluid dynamics [8,19,31,33,36]. Normally, they are determined considering the plug-flow approach [2,16,28,29,46,55,56,58,60–63].
- Experimental observations in absence of reaction and non-weighted regression are used for the estimation of h_w and $k_{eff,r}$, presenting a high statistical correlation [8,16,31,46,58,61,64], making them unreliable for modeling purposes.
- Temperature gradients generated during experiments in absence of reaction for determining the heat transfer parameters are lower than those observed under reaction conditions [16,28,43,46,54,55,65].
- When neglecting the use of h_w, an effective thermal conductivity is determined but the effect of fluid dynamics on this parameter is neglected [65,66]. Moreover, the effect of the external wall (coolant side) heat transfer resistance on temperature profiles is neglected.

In the present work, a generalized approach to model heat transfer in a wall-cooled packed bed reactor with low d_t/d_p is proposed and assessed accordingly. This approach overcomes the limitations outlined above, by implementing experimental and theoretical methodologies for adequately accounting for fluid dynamics and radial heat transfer. Temperature gradients, similar to those observed in industrial-scale reactors, are experimentally assessed in order to determine the heat transfer parameters following the pseudo-local approach and weighted regression. The developed approach for determining the radial effective thermal conductivity accounts for the effect of fluid dynamics on the pseudo-locality of the radial heat transfer from the core of the bed to the wall; it aims at improving the heat transfer modeling within the packed bed reactor, particularly in those zones presenting high void fractions, including the wall zone. Furthermore, the adequate description of the heat transfer at both the internal and external wall of the reactor tube allows for the reliable determination of the heat transfer resistances encountered at the external side of the packed bed reactor, resulting from the heat exchange between the coolant fluid and the packed bed. The developed approach is compared with the conventional heat transfer modeling approaches which are generally applied to describe the performance of highly exothermic reactions in packed bed reactors with a d_t/d_p lower than 8 $m_r\ m_s^{-1}$. To this end, the impact of each heat transfer approach examined here is evaluated during the modeling of a wall-cooled industrial-scale packed bed reactor.

Oxidative dehydrogenation of ethane (ODH-C_2) over a V-based multi-metallic catalyst is taken as the case study to demonstrate the methodology for several reasons. Firstly, it is a promising alternative reaction in the petrochemical industry for ethylene production. It becomes relevant with the advent of the first pilot reaction unit, of which, as far as authors know, the design was confirmed after lab and pilot phase validations in 2017 [67]. ODH-C_2 has several advantages, such as low energy consumption, low CO_x production and high selectivity to ethylene, compared to the conventional process, i.e., steam cracking of hydrocarbons and fluid-catalytic cracking of gas oils [68]. Secondly, works from literature and some contributions from our research group have demonstrated that V-based multi-metallic materials are, nowadays, some of the most promising catalysts because of their high ethane reactivity at relatively low temperatures, i.e. below 500 °C, and high selectivity to ethylene [3,31,69]. Additionally, an intrinsic kinetic model following the Eley-Rideal formalism from our research group is available [3]. Consequently, relevant industrial-scale reactor simulations targeting the elucidation of the advantages of the proposed approach are presented in this work, along with a comparison with the conventional heat transfer approximations.

2. Procedures

The experimental set-ups used in this work are a bench and industrial-scale single-tube packed bed with a tube-to-particle diameter ratio of ~3 $m_r\ m_s^{-1}$ packed with spherical pellets of a V-based active phase supported on TiO_2 in its anatase phase. The effective diameter of the pellets amounts to 0.0082 m_s. Pressure drop and temperature gradients in absence of reaction are measured under industrially relevant conditions in these packed beds in order to characterize fluid dynamics and the heat transfer, respectively. A pseudo-local heat transfer approach is developed and further evaluated during the modelling of an industrial-scale wall-cooled packed-bed catalytic reactor for ODH-C_2.

The procedures are organized into four sections. Section 2.1 presents the experimental set-ups and the operating conditions at which both the pressure drop, and temperature gradient experiments are performed. Section 2.2 provides a detailed approach for simulating fluid dynamics where solid-fluid interactions at the center of the bed are characterized by determining the apparent permeability constants (K and K_z), while the solid-fluid and fluid-fluid interactions close to the wall are quantified by determining the effective viscosity (μ_{eff}). Section 2.3 introduces the experimental and theoretical methodology to characterize the radial heat transfer in the wall-cooled packed bed reactor. The different heat transfer zones and the radial temperature gradient experiments are presented. Then, the pseudo-local approach developed in this work is introduced. The pseudo-local radial effective conductivity ($k_{eff,r,PLA}(r)$) is determined as a function of the radial void fraction and fluid dynamics. In addition, based on the adequate internal heat transfer characterization, the external wall heat transfer coefficient ($h_{w,ext}$) is characterized to capture the effect of the heat transfer resistances in the external heat boundary layer ($\delta_{HT,ext}$). Finally, Section 2.4 presents the numerical methods used to solve the models and perform the regression analyses.

2.1 Bench and industrial scale packed bed reactor

A schematic diagram, representative for both the bench and the industrial-scale packed bed reactor, is shown in Figure 1. The different ways in which the reactor set-up can be operated, depending on which information is pursued, i.e., pressure-drop or temperature-gradient data, are depicted. The bench-scale packed bed is a tube, with a length of 0.5060 m_r and a diameter of 0.0254 m_r, surrounded by an electric resistance (the heat source) and covered by a thermal insulation jacket of fiberglass. The bed is packed with ca. 300 g (400 pellets) and 1.73 kg (2260 pellets) for the bench- and industrial-scale packed bed reactor, respectively. The pellets are spherical catalyst particles with a diameter of 0.0082 m_s. These particles are composed of a V-based active phase externally deposited on a TiO_2 (anatase) core. Manometers are positioned at both the inlet and outlet of the packed bed in order to measure the pressure drop along the bed. The temperature is measured with 0.1 mm outside diameter K-type thermocouples (not shown so as not to overload Figure 1) at different axial positions in the packed bed, through thermowells from the side. The thermocouples are set up such that they can be moved over the entire diameter of the packed bed. One thermocouple is positioned at mid-height of the reactor at the tube wall as a control set point to generate the required temperature gradients. This configuration allows the measurement of radial and axial temperature gradients.

The industrial-scale wall-cooled packed bed is a tube with a length of 2.6 m and a diameter of 0.025m surrounded by a molten salt bath. The bed is packed with the same pellets used in the bench-scale system. The pressure drop from the inlet to the outlet of the packed bed is, again, measured using two manometers. Platinum resistance thermometers and 1.5 mm outside diameter chromel-alumel sheathed thermocouples are used to measure the temperature from the wall to the center of the packed bed at different axial positions [13]. In this packed bed system, the coolant temperature is monitored during the experimentation.

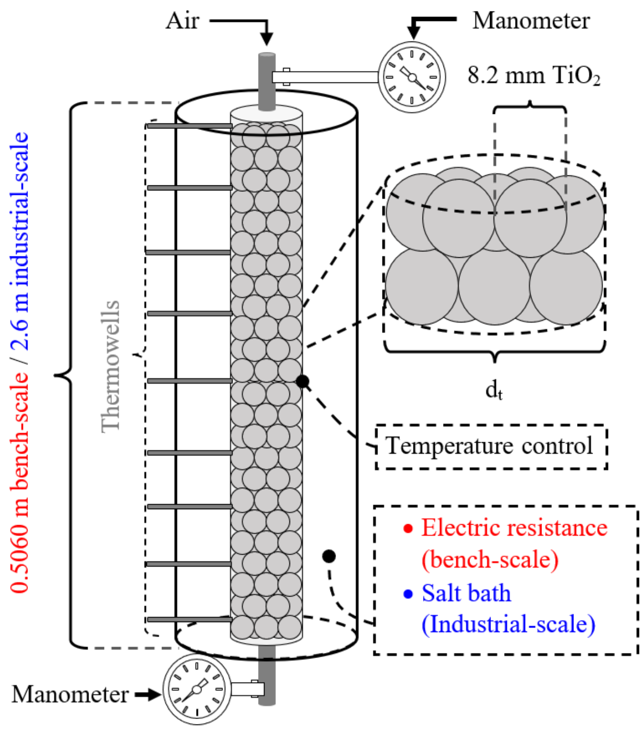

Figure 1. Schematic diagram of the packed bed showing the different kind of operations depending on the targeted variables. Industrial-scale and bench-scale operation and bed length in blue and red, respectively.

2.2 Fluid dynamics

2.2.1 Pressure drop

Pressure drop experiments, performed in the bench-scale reactor, consisted of measuring the pressure at the inlet and outlet of the bed for a particle Reynolds number (Re_p) between 210 and 1680, evaluated at normal conditions. Pressure drop experiments in the industrial-scale reactor were obtained at a Re_p between 750 and 1750, evaluated at normal conditions [13].

Pressure drop in packed beds is caused by frictional energy losses. These energy losses are caused by viscous frictional resistances, particularly at low flow rates, which have a linear relationship with the flow velocity (Blake-Kozeny equation [70]), and inertial frictional resistances, which have a quadratic relationship with the flow velocity (Burke-Plummer equation [71]). Ergun [53] demonstrated that the summation of the expressions for the low and high-velocity ranges provides an expression for the entire range of volumetric flow rate. This leads to Ergun's equation where the pressure drop along the axial coordinate ($\Delta P_z/L$) can be seen for the studied bed as the z-component of the solid-fluid resistance vector [72], **D(r)**:

$$\frac{\Delta P_z}{L} = D(r)_z = \alpha \frac{u_z \mu_f}{d_p^2} \frac{(1-\varepsilon(r))^2}{\varepsilon(r)^3} + \beta \frac{\rho_f u_z^2}{d_p} \frac{(1-\varepsilon(r))}{\varepsilon(r)^3} \tag{1}$$

or, expressed in function of the apparent permeability:

$$D(r)_z = \mu_f H(r)_{zz}^{-1} u_z \tag{2}$$

where u_z is the axial superficial velocity, μ_f is the fluid viscosity, ε is the radial void fraction averaged at the axial and tangential axis, $H(r)^{-1}_{zz}$ is the axial component of the apparent permeability tensor (**H(r)**), and α and β are two constants related to the viscous and inertial terms, respectively. Because these contributions are different for each system, i.e., the geometrical configuration attributed to the shape and size of the packings and the d_t/d_p ratio, α and β are re-estimated based on the experimentally measured pressure drop. The re-estimation of α and β allows determining the Darcy and Forhheimer permeabilities, presented in Eqs. (3) and (4), respectively.

$$K = \frac{\varepsilon(r)^3 d_p^2}{\alpha(1-\varepsilon_0)^2} \tag{3}$$

$$K_z = \frac{\varepsilon(r)^3 d_p}{\beta(1-\varepsilon(r))} \tag{4}$$

These terms provide information about the inertial and viscous resistances caused by the solid-fluid interactions. In addition, K and K_z allow the determination of the Darcy (Da) and Forchheimer (Fo) numbers, see Eqs. (5) and (6), respectively. Da provides information of the influence of the viscous term due to frictional energy losses from fluid-fluid and solid-fluid interactions, while Fo gives details of the inertial resistances within the packed bed [33,51,73,74].

$$\mathrm{Da} = \frac{\mathrm{K}}{\mathrm{R_t^2}} \tag{5}$$

$$\mathrm{Fo} = \frac{\mathrm{K_z}}{\mathrm{R_t}} \tag{6}$$

2.2.2 Fluid dynamics model accounting for the mass conservation

The governing equations to model momentum transfer within the packed bed with low tube-to-particle diameter ratio are given by the continuity equation, see Eq. (7), and the Navier-Stokes-Darcy-Forchheimer equation following Brinkman's approach (BDF) where an effective viscosity (μ_{eff}) is introduced to characterize solid-fluid interactions close to the wall [75], see Eqs. (8) – (13).

Continuity equation:

$$\frac{\partial \mathrm{v_z}}{\partial \mathrm{z}} = 0 \tag{7}$$

Momentum equation:

$$\rho_f\left[\frac{\partial \mathrm{v_z}}{\partial \mathrm{t}} + \varepsilon(\mathrm{r})\mathrm{v_z}\frac{\partial \mathrm{v_z}}{\partial \mathrm{z}}\right] = -\varepsilon(\mathrm{r})\frac{\partial \mathrm{p_z}}{\partial \mathrm{z}} + \mu_{eff}\nabla^2\varepsilon(\mathrm{r})\mathrm{v_z} - \left(\frac{\mu_f}{\mathrm{K}}\varepsilon(\mathrm{r})\mathrm{v_z} + \frac{\rho_f}{\mathrm{K_z}}\varepsilon(\mathrm{r})^2\mathrm{v_z^2}\right) + \varepsilon\rho_f \mathrm{g_z} \tag{8}$$

The initial and boundary conditions are:

$$\mathrm{t} = 0 \qquad \mathrm{v_z} = \mathrm{v_{z,ss}} \tag{9}$$

$$\mathrm{r} = 0 \qquad \frac{\partial \mathrm{v_z}}{\partial \mathrm{r}} = 0 \tag{10}$$

$$\mathrm{r} = \mathrm{R_t} \qquad \mathrm{v_z} = 0 \tag{11}$$

$$\mathrm{z} = 0 \qquad \mathrm{v_z} = \mathrm{u_{z,0}} \tag{12}$$

$$\mathrm{z} = \mathrm{L} \qquad \frac{\partial \mathrm{v_z}}{\partial \mathrm{z}} = 0 \tag{13}$$

The left side of Eq. (8) describes the inertial forces due to fluid-fluid interactions. On the right side, the first term accounts for the pressure drop within the bed (pressure forces), the second term describes the radial viscous dissipation, including the use of an effective viscosity

(μ_{eff}), proposed by Brinkman [75], to account for the impact of solid surfaces, associated with the wall and the packing on fluid dynamics in the region near the wall of the bed. The third term contains the Darcy and Forchheimer contributions. These terms describe the viscous and inertial solid-fluid interactions in the packed bed, respectively. The last term captures the gravitational forces. The void fraction profile within the bed is obtained by following the correlation developed by De Klerk [76] for packed beds with $d_t/d_p < 8$ containing spheres.

Since the pressure drop and the void fraction can be determined with high certainty, an accurate description of velocity profiles in a packed bed with low tube-to-particle diameter ratio depends on determining three parameters, the so-called fluid dynamic descriptors, i.e., μ_{eff}, α and β. As mentioned above, α and β can be estimated from pressure drop data for the further determination of K and K_z. Determining μ_{eff} is more challenging. Although a continuity equation is stated when presenting the fluid dynamic model, in the literature approaches [50,51,77,78] mass conservation is not accomplished, i.e., the mass flux at any axial position in the bed can deviate from the mass flux at the inlet of the system. To overcome this shortcoming, a conservative methodology aimed at determining μ_{eff} is proposed here to describe the fluid dynamics within packed beds with a tube-to-particle diameter ratio smaller than 8 $m_r\ m_s^{-1}$ by forcing the momentum equation to meet the continuity equation by fitting the mass flux with the observed one at the bed inlet. Firstly, the superficial velocity (u_z) at any axial position in the packed bed is obtained by determining the interstitial velocity (v_z) and multiplying it with the void fraction within the bed (ε_i), see Eq. (14).

$$u_z = v_z \varepsilon_i \tag{14}$$

Then, the average superficial velocity, i.e., the result of dividing the volumetric flow by the cross-sectional area where the fluid flows, is calculated as follows:

$$\langle u_z \rangle = \frac{\int_0^{2\pi} \int_{r=0}^{r=R_t} v_z r \, dr \, d\theta}{\int_0^{2\pi} \int_{r=0}^{r=R_t} r \, dr \, d\theta} \quad (15)$$

Eq. (15) can be solved using weighted orthogonal collocation, resulting in Eq. (16) for the superficial velocity:

$$\langle u_z \rangle = \sum_{i=1}^{N} W_i \varepsilon_i v_{z,i} \quad (16)$$

where W_i is the weight factor assigned to the i-th collocation point, $v_{z,i}$ is the interstitial velocity, ε_i is the void fraction and N is the number of radial collocation points. Once the average superficial velocity is calculated, the mass flux at any axial position within the bed can be calculated as follows:

$$G = \rho_f \langle u_z \rangle \quad (17)$$

μ_{eff} is, then, ultimately determined via regression, while ensuring mass conservation along the bed. It is worth mentioning that this approach allows the determining the μ_{eff} without the need for interstitial velocity measurements.

2.3 Radial heat transfer in absence of reaction

To overcome the limitations mentioned in the introduction when determining $k_{eff,r}$ and h_w, an alternative methodology to characterize the radial heat transfer mechanisms is proposed here by considering a pseudo-local approach accounting for a pseudo-local radial effective conductivity, $k_{eff,r,PL}(r)$, and an external heat wall transfer coefficient, $h_{w,ext}$. This “pseudo-local approach” is benchmarked against the conventional approaches reported in the literature. Additionally, the experimental methodology aims at determining temperature gradients similar to those observed in industrial-scale wall-cooled packed-bed reactors. Observations are used to estimate the heat transfer parameters for each approach, the one proposed in this work and the more conventional ones. The estimation of the heat transfer parameters is performed using weighted regression focusing on the temperature gradients at the core of the bed and near the wall. In order to provide a decoupled assessment of the contribution of heat transfer mechanisms to the overall performance of the packed bed, different radial zones are identified in the packed and analyzed in the next sections.

2.3.1 Radial heat transfer zones

Figure 2 displays the different radial heat transfer zones in the packed bed by showing temperature profiles in each zone qualitatively. The tube thickness, represented by a black line between the wall zone and the external boundary layer zone, has no significant effect on the radial heat transfer resistances because of the sufficiently high thermal conductivity of the tube material, i.e., stainless steel.

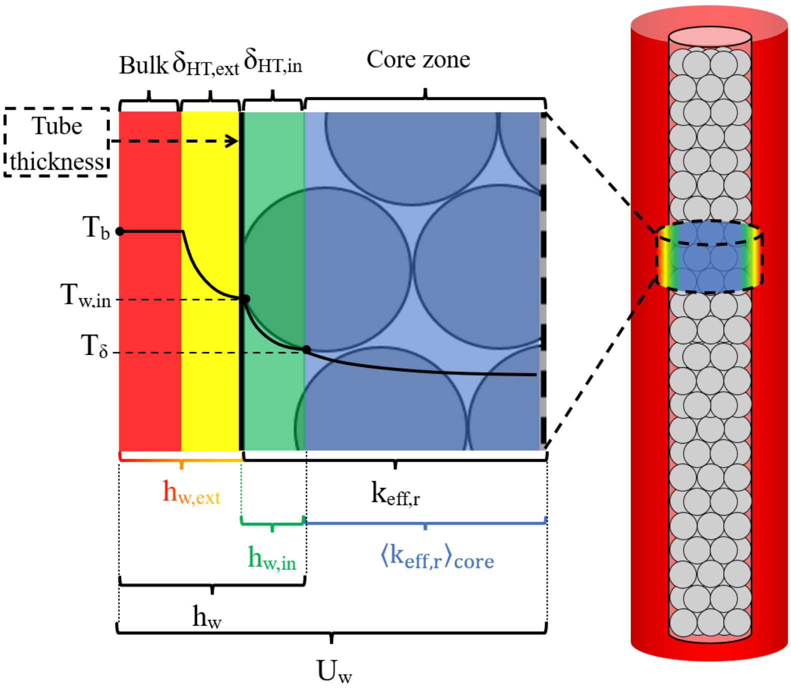

Figure 2 Schematic diagram of the relevant radial zones in a packed bed: core zone (blue), internal wall zone (green), external wall zone (yellow) and heat transfer medium (red).

Four different zones can be identified as a function of the radial coordinate. Each of these zones relates to an effective heat transfer parameter, such that each zone presents a characteristic temperature gradient which can be associated with a corresponding heat transfer mechanism. The core zone (blue) spans from the center of the bed to the heat boundary layer near the internal tube wall. In this region, the radial heat transfer mechanisms are captured by $k_{eff,r}$. In the wall zone (green), an internal heat pseudo-boundary layer, $\delta_{HT,int}$, may generate a significant heat transfer resistance enhancing the temperature gradient, i.e., the temperature difference between T_δ and $T_{w,in}$. In this heat pseudo-boundary layer, the heat transfer is described by $h_{w,int}$. An external heat pseudo-boundary layer ($\delta_{HT.ext}$) generates another temperature gradient, at the external surface of the reactor tube. In this zone, $h_{w,ext}$ quantifies the temperature gradient between $T_{w,in}$ and T_b. This is one of the key differences between our work and previously reported ones. In the literature, no distinction is made between the internal and external heat pseudo-boundary layer and h_w is modeled as a single parameter that captures the heat transfer mechanisms in both zones, i.e., internal and external wall zones. Lastly, the coolant zone (red) represents the zone where the heat source/sink for the packed bed is situated and it can be assumed that there are no significant temperature gradients in this zone because of the mixing in it [5,13].

2.3.2 Radial temperature gradient experiments

The heat transfer experiments, aiming at determining the heat transfer parameters, are performed by heating the bench-scale packed bed with an electric resistance around the external surface of the tube while air is fed from the top of the packed bed [16,36,46,60,61]. This generates not only significant axial, but also radial temperature gradients, similar in magnitude to those identified in industrial packed bed reactors. Inlet air flow rates corresponding to a Re_p between 210 and 1260 at normal conditions are used during heat transfer experimentation. For the bench-scale packed bed, the temperature was measured at twelve and nine, radial an axial positions, respectively. While for the industrial-scale, the temperature was measured at three axial positions and different radial positions depending of the inlet flow rate, i.e., at seventeen, thirty three and eight radial positions at Re_p of 1400, 1050 and 700, respectively. These observations are obtained with a salt bath as the heat source (or the coolant fluid). At all air flow rates, heat transfer experiments are carried out by using a coolant temperature of 400 °C. The observed temperature gradients are then used to estimate the parameters from the radial heat transfer mechanisms.

Through the development of a pseudo-continuous model for a packed bed, the use of a pseudo-local approach accounting for the role of the velocity profile on radial heat transfer has led to a better understanding and characterization of the radial heat transfer mechanisms, mainly in the wall zone [4,12,65,81,82]. Nevertheless, the pseudo-locality itself has not been adequately assessed such that fluid dynamics has not been properly considered during the determination of a pseudo local $k_{eff,r}$ (hereafter called $k_{eff,r,PLA}(r)$). Typically, a plug flow approach has been considered in the literature [1–3,27–29,31,37,44–46]. When fluid dynamics is included, $k_{eff,r,PLA}(r)$ remains constant in the core zone, where the lowest temperature gradients occur, while in the internal wall zone the $k_{eff,r,PLA}(r)$ starts to decrease linearly. Additionally, the estimation of the pseudo-local parameters has been performed at adiabatic conditions[65], or considering an uniform static thermal conductivity, $k^0_{eff,r}$ in the core zone and the fluid thermal conductivity as the $k_{eff,r}$ in the wall zone [81]. To this end, the approach developed in this work not only allows the characterization of the internal heat transfer mechanisms by determining a pseudo-local $k_{eff,r,PLA}(r)$, but also the heat transfer mechanisms at the external surface of the tube by determining the $h_{w,ext}$.

Firstly, the pseudo-homogeneous heat transfer model used to describe the radial temperature profiles within the packed bed is presented as follows:

$$(\rho_s Cp_s + \rho_f Cp_f)\frac{\partial T}{\partial t} + \rho_f Cp_f \varepsilon v_z \frac{\partial T}{\partial z} = \frac{1}{r}\frac{\partial}{\partial r}\left[k_{eff,r,PLA}(r) r \frac{\partial T}{\partial r}\right] + k_{eff,z}\frac{\partial^2 y}{\partial z^2} \tag{18}$$

$$t = 0 \qquad T(0, r, z) = T_{ss} \tag{19}$$

$$z = 0 \qquad v_z \rho_f Cp_f (T_0 - T) = -k_{eff,z}\frac{\partial T}{\partial z} \tag{20}$$

$$z = L \qquad \frac{\partial T}{\partial z} = 0 \tag{21}$$

$$r = 0 \qquad \frac{\partial T}{\partial r} = 0 \tag{22}$$

$$r = R_t \qquad T = T_{w,in}(z) \tag{23}$$

The first term on the left-hand side of Eq. (18) is the accumulation term while the second is the convective one where fluid dynamics plays a significant role. The term on the right-hand side is the radial conductive term where the pseudo-local $k_{eff,r,PLA}(r)$ captures the static and dynamic internal radial heat transfer mechanisms. The assumptions considered in this model are: (i) a pseudo-local thermal equilibrium between solid and fluid phases, (ii) Newtonian and incompressible fluid within the packed bed, and (iii) constant physical properties of the fluid. It should be noted that commonly the axial effective conductivity ($k_{eff,z}$) is neglected when modelling packed bed reactors. However, because proper analysis of its impact on the radial heat transfer mechanisms is beyond the contribution of this paper, research on the axial conductivity on low d_t/d_p packed beds will be provided in further work.

The boundary condition from Eq. (23), referred to as the known wall-temperature boundary condition (KWT-BC), allows the characterization of the internal heat transfer mechanisms in the packed bed. Following the mathematical equations proposed by the group of Vortmeyer [65,82], see Eqs. (24) and (25), the pseudo-local radial effective conductivity, $k_{eff,r,PLA}(r)$, can be determined accounting for fluid dynamics.

$$k_{eff,r,PL}(r) = k^0_{eff,r} + k_{1,h} Pr Re_p [f(R_t - r)] k_f + \tag{24}$$

$$f(R_t - r) = \begin{cases} \left(\frac{R_t - r}{k_{2,h} d_p}\right); & \text{for } 0 < R_t - r \le k_{2,h} d_p \\ 1 \quad ; & \text{for } k_{2,h} d_p < R_t - r \le R_t \end{cases} \tag{25}$$

Here $k^0_{eff,r}$ is the static radial effective conductivity, i.e., when the Re_p approaches 0, $k_{1,h}$ is the constant impacting on the dynamic contribution of the $k_{eff,r,PL}(r)$, $k_{2,h}$ is the damping parameter that determines where the pseudo-local $k_{eff,r,PLA}(r)$ decreases due to the effect of the internal heat pseudo-boundary layer, $\delta_{HT,in}$, and k_f is the fluid thermal conductivity. Hereafter, this approach is referred as the Pseudo-local Internal Heat Transfer Approach (PL-IHTA).

Additionally, the reproduction of the temperature profiles in absence of reaction from the PL-IHTA are compared with the conventional state-of-the-art approach, i.e., Boundary Layer Approach considering the KWT-BC, here referred as the KWT-BLA. For the sake of brevity, the details of KWT-BLA are given in Section A in Supporting information.

Since the pseudo-local $k_{eff,r,PLA}(r)$ can be determined from the PL-IHTA, the following boundary condition is proposed for the estimation of the $h_{w,ext}$:

$$r = R_t \qquad -k_{eff,r,PLA}(r)\frac{\partial T}{\partial r} = h_{w,ext}\left(T_{w,in} - T_b\right) \tag{26}$$

In the following, this approach is referred to as the pseudo-local approach (PLA). PLA helps to understand the role of the heat transfer mechanisms in the high void fraction zones and provides quantitative information of the internal heat boundary layer. Moreover, PLA avoids the historical cross-correlation issue between $k_{eff,r}$ and h_w because the pseudo-local $k_{eff,r,PLA}(r)$ is obtained separately from $h_{w,ext}$.

With the pseudo-local $k_{eff,r,PLA}(r)$ and $h_{w,ext}$ estimated, a resistance analysis for the different zones is developed as follows [83]:

$$\frac{1}{U_w} = \frac{1}{h_{w.ext}} + \frac{R_t}{4k_{eff,r,PLA}(r)} \tag{27}$$

where U_w is the overall heat transfer coefficient, the internal heat transfer resistances are characterized by the pseudo-local $k_{eff,r,PLA}(r)$, and the external heat transfer resistances are characterized by $h_{w,ext}$. The $h_{w,ext}$ is estimated via Eq. (26), while $k_{eff,r,PLA}(r)$ is estimated from Eqs. (24) – (25).

2.3.3 Heat transfer under reaction conditions

The performance of a multitubular wall-cooled packed bed reactor is normally predicted by assuming that a single tube operates the same as the rest of the tubes [84–86]. Thus, the performance of an industrial-scale single tube wall-cooled packed bed reactor operating in a non-isothermal and non-adiabatic mode is simulated here. As mentioned earlier, the ODH-C_2 is considered as the case study for the reactor simulations. The ODH-C_2 kinetics have been described in our research group [3,69] for a multi-metallic V-based catalyst supported on TiO_2 following an Eley-Rideal mechanism. For the sake of brevity, the details of the kinetics are given in Section B in Supporting Information.

The reactor model is constructed while accounting for fluid dynamics, because of its effect on the heat transfer mechanisms within the bed, including its effect on the pseudo-local effective heat transfer parameters. To this end, heat and mass transfer mechanisms are accounted for in a pseudo-heterogeneous two-dimensional model, based on averaged general conservation relations, yet, by considering effective transport parameters:

Gas phase

$$\varepsilon \frac{\partial \mathrm{C_n}}{\partial \mathrm{t}} + \varepsilon \mathrm{v_z} \frac{\partial \mathrm{C_n}}{\partial \mathrm{z}} = \varepsilon\, \mathrm{D_{eff,z}} \frac{\partial^2 \mathrm{C_n}}{\partial \mathrm{z}^2} + \varepsilon\, \mathrm{D_{eff,r}} \left[\frac{\partial^2 \mathrm{C_n}}{\partial \mathrm{r}^2} + \frac{1}{\mathrm{r}}\frac{\partial \mathrm{C_n}}{\partial \mathrm{r}}\right] + (1-\varepsilon)\mathrm{k_g a_s}\left(\mathrm{C_{n,s}} - \mathrm{C_n}\right) \tag{28}$$

$$\varepsilon \rho_\mathrm{f} \mathrm{C_{p,f}} \frac{\partial \mathrm{T}}{\partial \mathrm{t}} + \varepsilon \mathrm{v_z} \rho_\mathrm{f} \mathrm{C_{p,f}} \frac{\partial \mathrm{T}}{\partial \mathrm{z}} = \mathrm{k_{eff,z}} \frac{\partial^2 \mathrm{T}}{\partial \mathrm{z}^2} + \frac{1}{\mathrm{r}}\frac{\partial}{\partial \mathrm{r}}\left[\mathrm{k_{eff,r,PLA}}(r) r \frac{\partial \mathrm{T}}{\partial \mathrm{r}}\right] + (1-\varepsilon)\mathrm{h_g a_s}(\mathrm{T_s} - \mathrm{T}) \tag{29}$$

Solid phase

$$(1-\varepsilon)\frac{\partial \mathrm{C_{n,s}}}{\partial \mathrm{t}} = (1-\varepsilon)\mathrm{k_g a_s}\left(\mathrm{C_n} - \mathrm{C_{n,s}}\right) + \rho_\mathrm{b} \sum_{\mathrm{i}=1}^{5} \nu_{n,i} \mathrm{r_i} \tag{30}$$

$$\rho_\mathrm{b} \mathrm{C_{p,s}} \frac{\partial \mathrm{T_s}}{\partial \mathrm{t}} = (1-\varepsilon)\mathrm{h_g a_s}(\mathrm{T} - \mathrm{T_s}) + \rho_\mathrm{b} \sum_{\mathrm{i}=1}^{5} (-\Delta H_i)\mathrm{r_i} \tag{31}$$

where C_n and $C_{n,s}$ are the molar concentration of the component *n* in the gas and solid phase, respectively, v_z is the interstitial axial velocity within the bed, $u_{z,0}$ is the inlet superficial axial velocity of the bed, T and T_s are the temperature in the gas and solid phase, respectively, $k_{eff,z}$ is the axial thermal conductivity and $k_{eff,r,PLA}(r)$ is the pseudo-local radial thermal conductivity.

The corresponding initial and boundary conditions are:

$$\mathrm{t} = 0;\ \mathrm{C_n} = \mathrm{C_{n,ss}} \text{ and } \mathrm{C_{n,s}} = \mathrm{C_{n,s,ss}} \tag{32}$$

$$\mathrm{t} = 0;\ \mathrm{T} = \mathrm{T_{ss}} \text{ and } \mathrm{T_s} = \mathrm{T_{ss}} \tag{33}$$

$$\mathrm{z} = 0;\ \mathrm{u_{z,0}C_{n0}} = \varepsilon\, \mathrm{v_z C_n} - \varepsilon\, \mathrm{D_{eff,z}} \frac{\partial \mathrm{C_n}}{\partial \mathrm{z}} \tag{34}$$

$$\mathrm{u_{z,0}} \rho_\mathrm{f} \mathrm{C_{p,f} T_0} = \varepsilon\, \mathrm{v_z} \rho_\mathrm{f} \mathrm{C_{p,f} T} - \mathrm{k_{eff,z}} \frac{\partial \mathrm{T}}{\partial \mathrm{z}} \tag{35}$$

$$\mathrm{z} = \mathrm{L};\ \frac{\partial C_n}{\partial z} = 0 \text{ and } \frac{\partial T}{\partial z} = 0 \tag{36}$$

$$\mathrm{r} = 0;\ \frac{\partial C_n}{\partial r} = 0 \text{ and } \quad \frac{\partial T}{\partial r} = 0 \tag{37}$$

$$\mathrm{r} = \mathrm{R_t};\ \frac{\partial C_n}{\partial r} = 0 \quad \text{ and } \quad \mathrm{k_{eff,r,PLA}(r)} \frac{\partial \mathrm{T}}{\partial \mathrm{r}} = \mathrm{h_{w,ext}}(\mathrm{T} - \mathrm{T_b}) \tag{38}$$

The reactor model, following the PLA is compared with the conventional state-of-the-art approaches, i.e., Classical Approach (CA) and Boundary Layer Approach (BLA) aiming at the elucidation of their limitations and providing the most reliable reactor model. For the sake of brevity, the details of CA and BLA are given in Section C in Supporting information.

2.4 Numerical methods

The reactor model is given in terms of a set of parabolic partial differential equations. Based on a mesh analysis, fluid dynamic, heat transfer and reactor models are discretized by the orthogonal collocation method using 40 and 15 points for the radial and axial positions, respectively, employing shifted Legendre polynomials [87]. The resulting set of ordinary differential equations is solved by a fourth-order Runge-Kutta-Fehlberg method [88].

The fluid dynamics parameters α, β and μ_{eff}, and the heat transfer parameters $k_{eff,r}$, $k_{eff,r,PLA}(r)$, h_w, $k_{1,h}$, $k_{2,h}$, $h_{w,ext}$, $h_{w,in}$, are estimated by a combination of weighted orthogonal distance regression [89] and the Levenberg-Marquardt algorithm [90] by the minimization of the following weighted objective function:

$$\mathrm{RSS}(\varphi) = \sum_{i=1}^{N} W_i \sum_{k=1}^{M} \left(F_{k,i} - \widehat{F_{k,\iota}}\right)^2 \xrightarrow{\varphi_1,\varphi_2,\ldots,\varphi_n} \min \tag{39}$$

where φ is the optimal parameter vector containing the adjustable parameters, N is the number of responses, W_i is the weight factor assigned to N, M is the number of independent observations, $F_{k,i}$ are the i experimental responses and $\widehat{F_{k,\iota}}$ are the predicted responses for the i independent observations. The initial guesses for the fluid dynamics and heat transfer parameters, when unknown, are chosen within the range of physically realistic values reported in the literature [15,36,53,65].

3. Results and discussion

3.1 Fluid dynamics

Results from the fluid dynamic characterization are presented in three sections: (i) Section 3.1.1 presents the estimation of α and β parameters related to the packed bed permeability via pressure drop experiments, (ii) Section 3.1.2 provides the results obtained in the determination of the packed bed permeability K and K_z, the Da and Fo numbers, as well as the apparent permeability, and (iii) Section 3.1.3 discusses the effect of considering mass conservation on the estimation of the μ_{eff} and the simulations of the velocity profiles.

3.1.1 Pressure drop – Viscous and inertial frictional forces

Figure 3 depicts the pressure drop observations and the simulation results using Eq. (1) with the parameters, α and β, estimated in this work as well as determined using some of the well-accepted correlations from literature [53,91,92]. Estimates for α and β and their confidence intervals are 2480 ± 447 and 2.31 ± 0.19, respectively. Simulations considering literature reported values for α and β [53,91–93] are not able to describe the experimental data acquired in the studied bed properly. This shows the importance of obtaining both parameters for a packed bed with low d_t/d_p. The estimated value of α and β are higher than the values reported in the literature [53,92,93]. The latter parameter is related to inertial forces which dominate at high flow rates. Thus, for the current case study, the inertial energy losses have a higher influence on the pressure drop than the viscous energy losses.

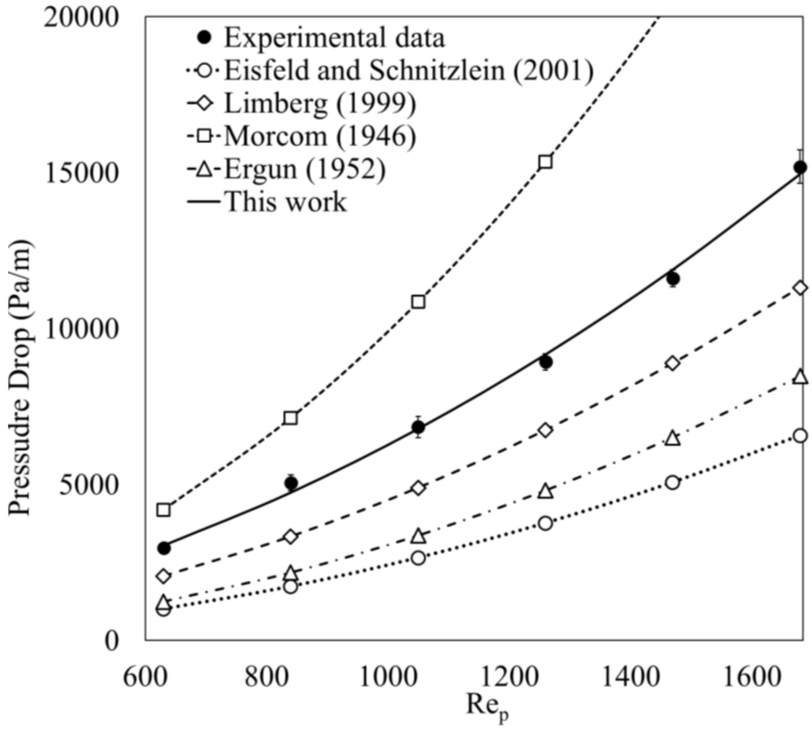

Figure 3. Pressure drop within the packed bed. A comparison between the experimental data (full symbols) and simulations with, the parameters estimated in this work (continuous line), Ergun's parameters [53] (α = 150 and β = 1.75), Limberg's parameters [91] (α = 260 and β = 0.9), Morcom's parameters [92] (green line, α = 245 and β = 2.4), and Eisfeld's correlation [93].

3.1.2 Void fraction, Darcy and Forchheimer number

Once α and β are obtained, the apparent permeability, and the Darcy (Da) and Forchheimer (Fo) numbers are determined. The void fraction is calculated using the correlation reported by De Klerk [76]. Figure 4a illustrates the Da and Fo numbers together with the void fraction within the bed for the bench-scale packed bed. Figure 4b depicts the apparent permeability within the packed bed.

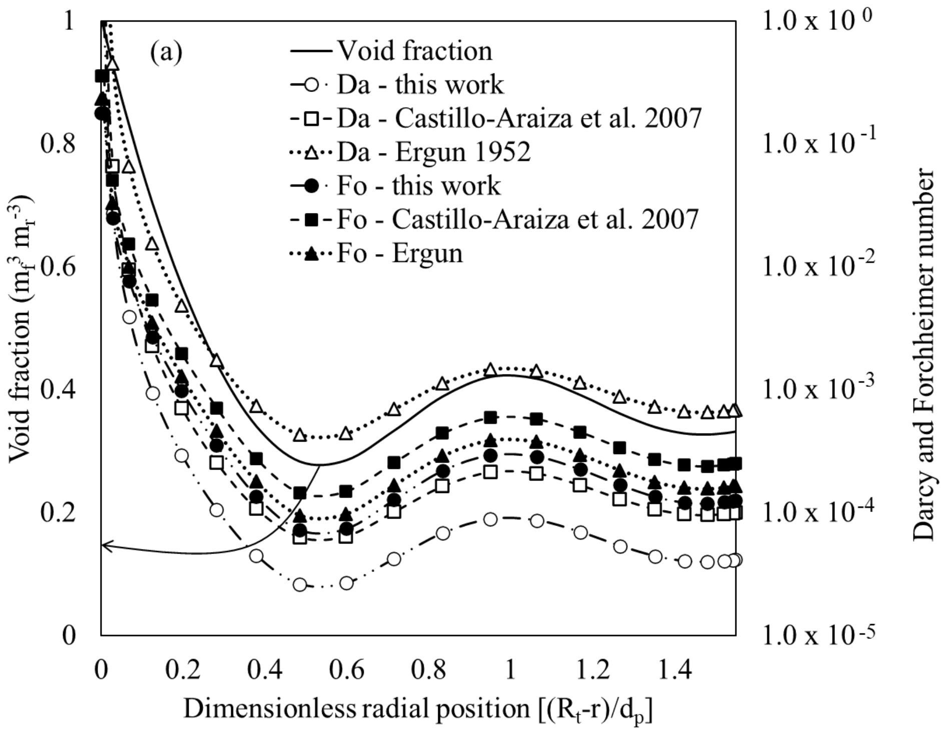

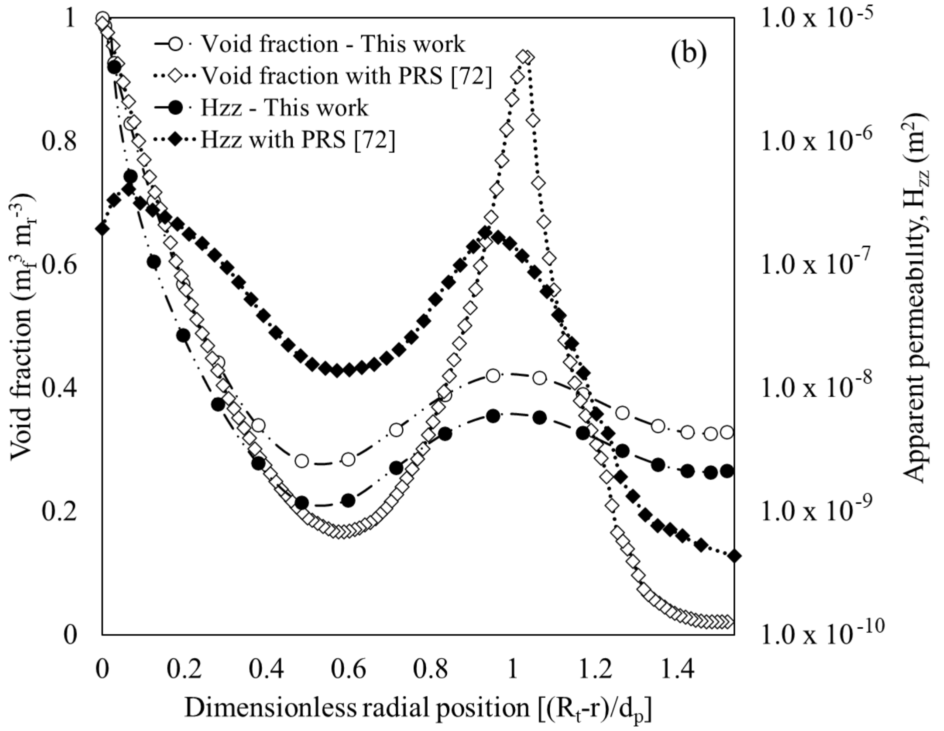

Figure 4. (a) Void fraction, Darcy and Forchheimer number for the bench and industrial-scale packed bed; and (b) Void fraction and apparent permeability in the packed bed obtained in this work and reported in the literature from a particle resolved simulation (PRS) [72].

The void fraction profile shows two zones with higher void fraction, i.e., near the wall and after one pellet-distance from the wall, where interstitial velocities are expected to be higher than the rest of the packed bed. The Da and Fo radial profiles present a similar trend to the void fraction profile. Da and Fo vary from 10^{-4} up to 10^{0} and 10^{-5} up to 10^{-2}, respectively, indicating that the inertial term, i.e., the Forchheimer permeability, and the Brinkman term should be considered in the fluid dynamic model. Otherwise, the impact of frictional energy losses on the fluid-fluid and solid-fluid interaction, i.e., non-Darcyan behavior, could not be properly accounted for. The apparent permeability determined in this work exhibits a similar trend as the one reported in the literature from particle resolved simulations (PRS) [72] for the same packed bed. However, a steeper increase in the wall zone and decrease in the center of the bed are identified. This is attributed to the methodology used to determine the apparent permeability, which in this work is calculated by using macroscopic pressure drop data through the estimation of α and β, while in PRS it is obtained by using local information. The agreement between the apparent permeability obtained here and the one reported in the literature, and the adequate prediction of the pressure drop observations provide confidence in the values of α and β estimated for quantifying the solid-fluid resistances at the core of the bed.

3.1.3 Velocity profiles - Effective viscosity

Figure 5 shows a comparison between the axial velocities at different particle Reynolds numbers considering the fluid dynamic models accounting and the ones not accounting [3,31] for the mass conservation criteria. Furthermore, the μ_{eff} was determined accounting for the mass conservation criterion. An overprediction of the velocity when μ_f is used is clearly observed in high void fraction zones, particularly, near the wall, because $\mu_f < \mu_{eff}$ at high Re_p. This means that fluid resistances are lower when μ_f is considered than when μ_{eff} is used, leading to the increment in velocity. Table 1 lists the estimated values of μ_{eff} along with the confidence intervals. μ_{eff} exceeds μ_f because the former captures the effect of the wall and packing surfaces on fluid dynamics along the radial direction of the bed. Moreover, μ_{eff} increases with the particle Reynolds number, in agreement with the literature [33,50,94].

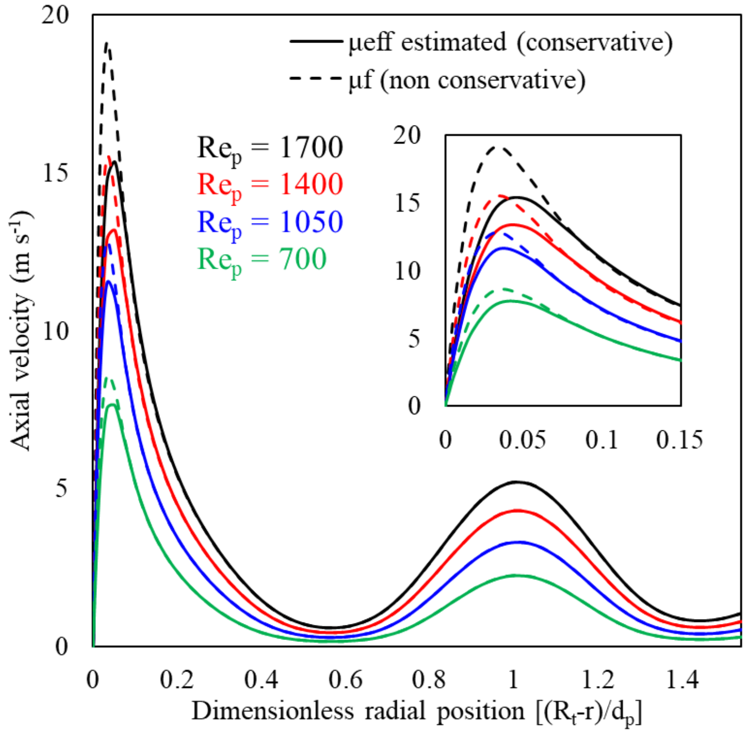

Figure 5. Axial velocity profiles within the packed bed. Re_p ranging from 700 to 1700.

Table 1. Estimated μ_{eff} values together with their 95% probability confidence intervals and the $\mu_{eff}/\ \mu_f$ ratio. Note that μ_f equals 222 $kg_f\ m_r^{-2}\ s^{-1}$.

Re_p	**μ_{eff} [$kg_f\ m_r^{-2}\ s^{-1}$]**	**$\mu_{eff}/\ \mu_f$**
210	222 ± 2.1	1.00
420	233 ± 2.4	1.05
630	246 ± 3.3	1.11
700	251 ± 3.6	1.13
1050	289 ± 5.4	1.30
1260	340 ± 5.0	1.53
1400	402 ± 5.6	1.81
1750	524 ± 6.8	2.36

3.2 Radial heat transfer

The results related of the radial heat transfer analysis are presented in four sub-sections: Section 3.2.1 presents the temperature profiles obtained from PL-IHTA versus those obtained from KWT-BLA. Section 3.2.2 provides the results for the radial heat transfer considering the

PLA, CA and BLA. Here, $k_{eff,r}$ and h_w are estimated for CA and BLA, while for PLA only $h_{w,ext}$ is estimated. Section 2.5.3.2.3 highlights the aspects of the heat transfer pseudo-locality by evaluating the effect of the void fraction, fluid dynamics and the internal heat pseudo-boundary layer. Additionally, the radial heat transfer resistances for the packed bed are presented.

3.2.1 Pseudo-local $k_{eff,r,PLA}(r)$

Figure 6 illustrates the capability of the PL-IHTA and KWT-BLA for describing radial and axial temperature profiles within the bench-scale packed bed at several Re_p. It should be noted that the temperatures at Re_p of 1260 are lower due to limitation of power on the electric resistance at this high flow. As can be seen, the PL-IHTA model can fit better to the experimental data than the KWT-BLA model, particularly in the wall zone. On the other hand, Figure 7 depicts the simulated industrial-scale packed bed temperature profiles using the PL-IHTA and KWT-BLA approaches with a coolant temperature of 400 °C and at Re_p of 1400. For sake of brevity, the radial temperature profiles are presented at one single axial position, i.e., 10 cm from the inlet. This is mainly because at this length the most challenging temperature gradients to describe are generated. However, it is possible to describe the radial temperature profiles at other lengths as well as the axial temperature profile, see Section D in Supporting Information. The estimated parameters for PL-IHTA and KWT-BLA are presented in Table 2 and Table 3, respectively. As expected, both parameters $k_{1,h}$ and $k_{2,h}$ follow the same trend for both the bench and industrial-scale packed bed. This is because the operating conditions, the d_t/d_p, and the packing geometrical configuration within both packed beds can be considered the same. These results demonstrate what is well known in the literature, an appropriate experimental design in a bench-scale packed bed allows an adequate internal heat transfer characterization which can be used for an accurate scale-up of the industrial-scale packed bed.

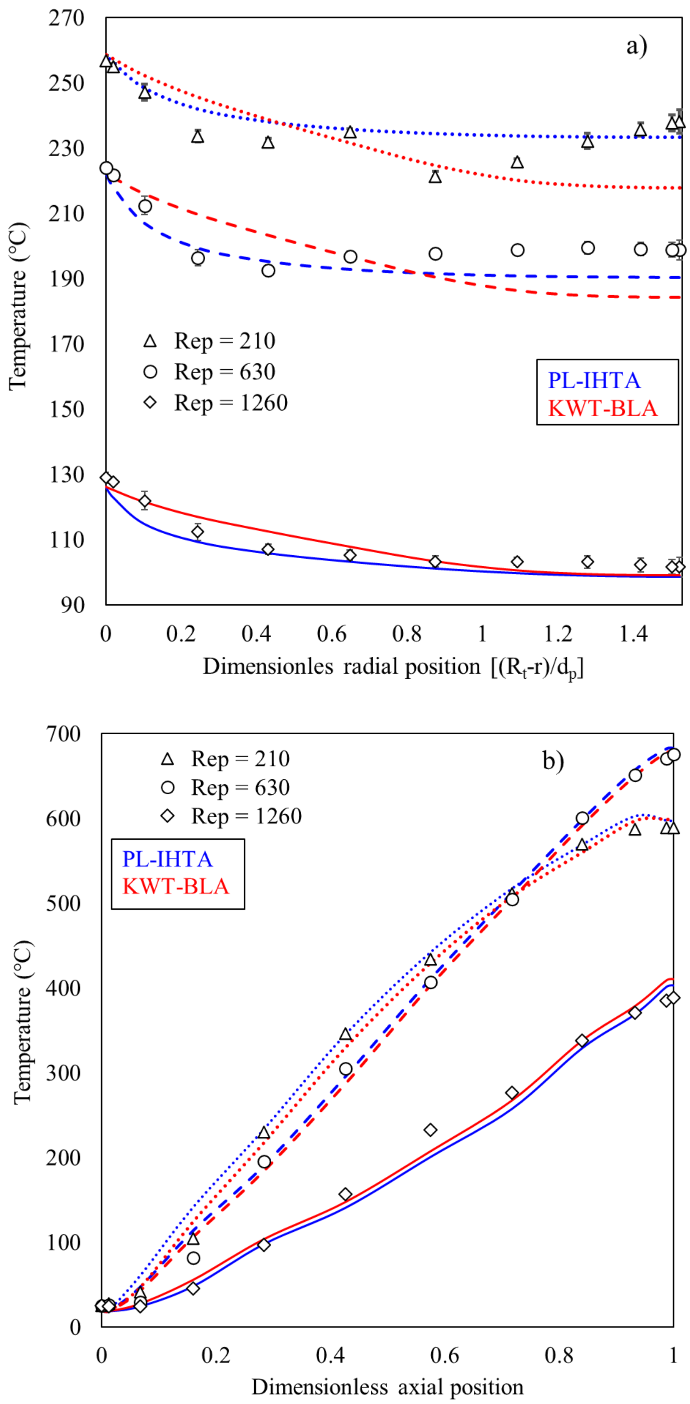

Figure 6. a) Radial temperature profiles at z = 13 cm from the inlet, and b) axial temperature profiles within a bench-scale packed bed. Comparison between the PL-IHTA and KWT-BLA at a Re_p of 210, 630 and 1260.

Table 2. Heat transfer parameter estimates and their corresponding 95% confidence intervals for the PL-IHTA (see Eqs. (24) – (25)).

Case	**Re_p**	**$k_{1,h}$**	**$k_{2,h}$**
PL-IHTA (Bench-scale)	210	0.56 ± 0.05	1.36 ± 0.12
	420	0.69 ± 0.05	1.20 ± 0.09
	630	0.96 ± 0.04	1.06 ± 0.10
	1260	5.34 ± 0.05	0.59 ± 0.04
PL-IHTA (Industrial-scale)	700	1.23 ± 0.08	1.10 ± 0.09
	1050	3.40 ± 0.07	0.71 ± 0.01
	1400	7.05 ± 0.05	0.52 ± 0.03

Table 3. $k_{eff,r}$ estimates and their corresponding 95% confidence intervals for the KWT-BLA (see Eqs. S1 – S6 in Supporting information)

Case	**Re_p**	**$k_{eff,r}$**
KWT-BLA (Bench-scale)	210	0.98 ± 0.07
	420	1.94 ± 0.19
	630	2.44 ± 0.23
	1260	2.81 ± 0.20
KWT-BLA (Industrial-scale)	700	2.31 ± 0.10
	1050	2.74 ± 0.09
	1400	2.66 ± 0.13

Note: $k_{eff,r}$ [=] W m^{-1} K^{-1}

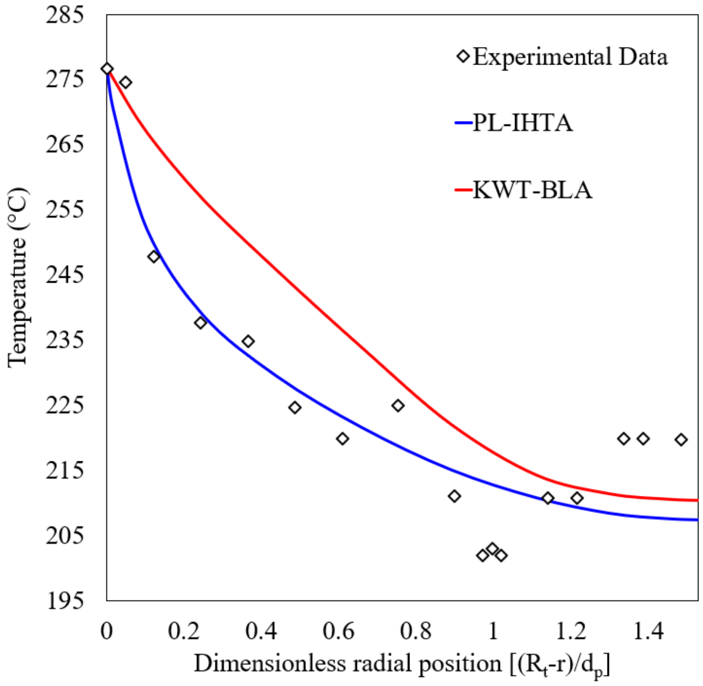

Figure 7. Comparison of the radial temperature profiles within an industrial-scale packed bed for the PL-IHTA and KWT-BLA models. Axial position: 0.10 m, Air flow rate corresponding to a Re_p of 1400.

Considering a pseudo-local $k_{eff,r,PLA}(r)$, when describing radial temperature observations, results in a major enhancement of the description of the temperature data along the radial axis, particularly in the wall zone. This improvement in the temperature description demonstrates the limitations of the conventional heat transfer approaches that consider $k_{eff,r}$. Figure 8 illustrates the pseudo-local variation of $k_{eff,r,PLA}(r)$ within the bench and industrial-scale bed for Re_p between 210 and 1400 with the void fraction profile as a reference. At all Re_p the trend is the same, there is a small decrease of the effective conductivity at the center of the bed, then a sudden rise in the high void fraction in the core zone, followed by a decrease after the high void fraction in the core zone and finally the effect of the $\delta_{HT,in}$ decreasing the $k_{eff,r,PLA}(r)$ value until the static contribution value at the tube wall. The $k_{eff,r,PLA}(r)$ captures heat transfer mechanisms when there is no flow, i.e., the static contribution, and when there is flow, i.e., the dynamic contribution [55,60,61]. In the static contribution, $k_{eff,r,PLA}(r)$ captures the thermal conduction through solids and the contact surface of the pellets, while in the dynamic contribution

$k_{eff,r,PLA}(r)$ captures the thermal conduction through the heat boundary layer near the pellets, heat transfer by convection between solid particles and by lateral mixing of the fluid. The results suggest that the dynamic heat transfer mechanisms are favored up to a Re_p of 630 in the core zone, after which a limit is reached such that the dynamic heat transfer mechanisms start to be affected, i.e., $k_{eff,r,PLA}(r)$ decreases as Re_p is increased up to 1400. This unexpected decrease of $k_{eff,r,PLA}(r)$ at high Re_p can be attributed to the synergy between the heat and fluid dynamics along the radial axis and axial convective mechanisms .

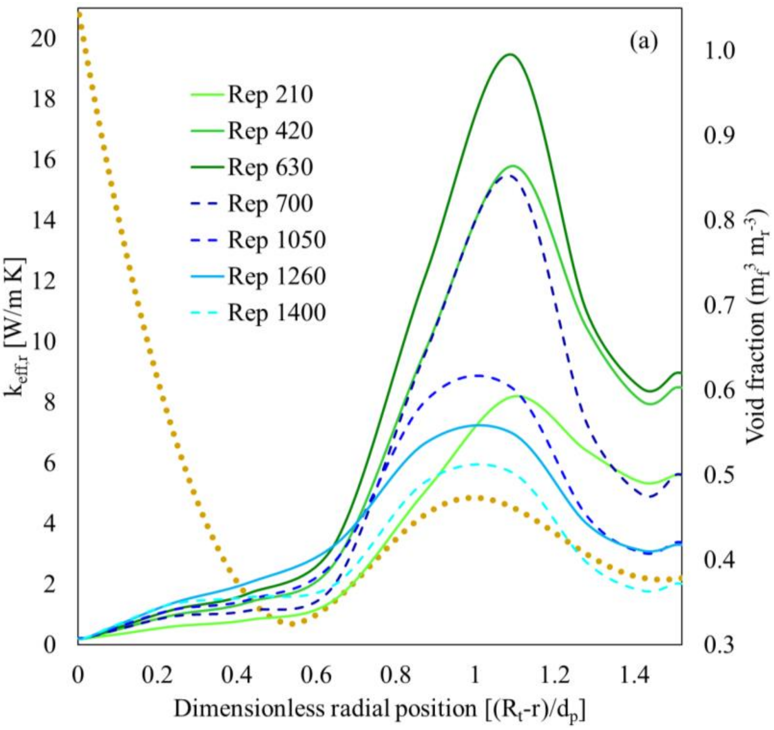

Figure 8. Pseudo-local $k_{eff,r,PLA}(r)$ within the packed bed at Re_p from 210 to 1400. Estimations performed in the bench-scale and industrial-scale packed bed are presented as continuous lines and dashed lines, respectively.

3.2.2 Characterization of the heat boundary layer: $k_{eff,r}$, h_w and $h_{w,ext}$

Figure 9 illustrates the radial temperature profiles predicted for the PLA, CA and BLA within the industrial-scale packed bed with a coolant temperature of 400 °C and Re_p between 700 and 1400. Temperature predictions are depicted at a length of 0.10 m from the bed inlet. It is worth noting that PLA, CA and BLA are the only approaches that can be used during the heat transfer modeling of an industrial-scale reactor, because they contain the effect of the coolant source, i.e., coolant or bath temperature, T_b. For modeling highly exothermic packed bed reactors in the literature [1,5,27,31,98], both the CA and the BLA are the state-of-the-art for characterizing radial heat transfer.

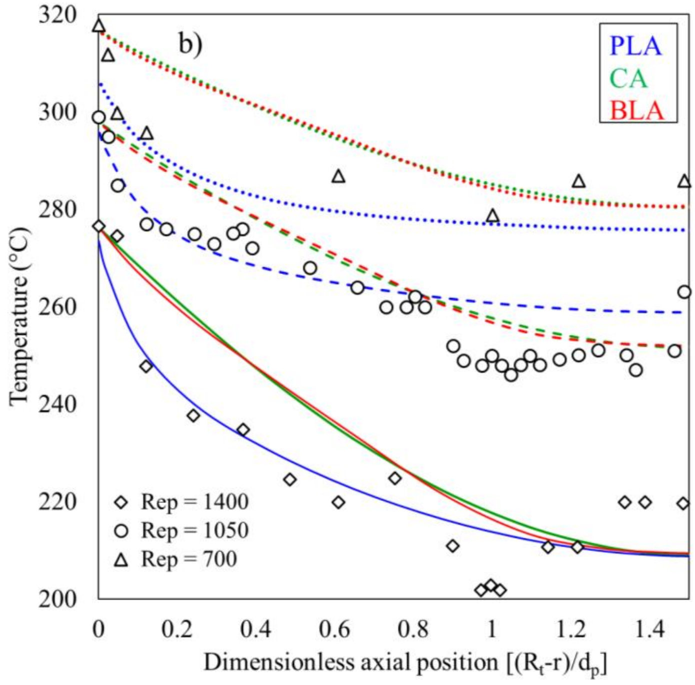

Figure 9. Radial temperature profiles within an industrial-scale packed bed for PLA, CA and BLA at 700 – 1400 Re_p.

As can be observed in Figure 9, the simulated temperature profiles considering the PLA are much closer to the experimentally observed ones, than when using the CA or BLA. The reliability of the PLA stems from several factors that, to the best of our knowledge, are not considered during the description of the radial heat transfer in the state-of-the-art literature [39,99]. Firstly, the use of the pseudo-local $k_{eff,r,PLA}(r)$ allows for a better understanding and characterization of the radial heat transfer mechanisms, mainly in the zones with high void fraction, including the wall zone (as shown in the next section). Thus, the parameters from the CA or the BLA cannot properly predict radial temperature profiles. Secondly, since fluid dynamics significantly impacts the magnitude of the radial heat transfer mechanisms, its modelling is essential to accurately determine the pseudo-local $k_{eff,r,PLA}(r)$. Moreover, in this work velocity profiles are modeled by considering a mass conservation criterion that allows determining the descriptors (α, β and μ_{eff}) which leads to a reliable modeling of fluid dynamics, as discussed in Section 3.1.

In contrast to the high cross-correlation between $k_{eff,r}$ and h_w, normally higher than 0.85 [8,16,31,46,58,61,64], when both parameters are estimated following the conventional approaches, i.e., the CA or the BLA, the cross-correlation obtained in this work was between 0.41 and 0.75 for the considered operating conditions, i.e., Re_p 700 – 1400. This is because the regression method applied in this work considers the effect of weights along the radial zone of the bed, which allows a proper description of the most pronounced temperature gradients, including those observed near the wall. On the other hand, the use of a pseudo-local $k_{eff,r,PLA}(r)$ not only provides a better reproduction of the experimental data and, hence, description of the radial heat transfer mechanisms, but also avoids the cross-correlation identified between $k_{eff,r}$ and h_w.

The parameters estimated for PLA, CA and BLA in an industrial-scale wall-cooled packed bed are presented in **Error! Reference source not found.**. For BLA, the $k_{eff,r}$ is re-estimated using the $k_{eff,r}$ obtained from the KWT-BLA as initial guess as it contains information of the heat transfer from the boundary layer which should be captured by h_w. Furthermore, the PLA can be used to obtain an averaged $k_{eff,r,PLA}(r)$ over the packed bed (see Section E in Supporting information) and use it as initial guess for the $k_{eff,r}$ re-estimation in BLA. When analyzing these parameters, it is worth noting that the wall heat transfer coefficient, h_w, obtained from the CA or the BLA captures the radial heat transfer resistances of a “negligible” heat boundary layer, as was shown in Figure 2. Moreover, because the boundary condition is set at the tube wall, $k_{eff,r}$ captures the radial heat transfer mechanisms from the center of the bed to the “negligible” heat boundary layer [15,16,46,64,81,95,100–106]. In contrast, the use of the pseudo-local $k_{eff,r,PLA}(r)$ allows properly characterizing the radial heat transfer resistances, such that the wall heat transfer coefficient, $h_{w,ext}$, is the only parameter estimated with the PLA. Thus, $h_{w,ext}$ captures the heat transfer mechanisms at the external side of the packed bed, i.e., the external heat pseudo-boundary layer.

Figure 10 depicts $k_{eff,r}$, h_w and $h_{w,ext}$ obtained for PL-IHTA, PLA, CA and BLA, along with parameter values calculated using correlations from the literature. All parameter estimates are within the order of magnitude reported in the literature. Nevertheless, the estimated $k_{eff,r}$ exhibits a sigmoidal trend instead of the reported linear trend. This might be related to the range of the Re_p assessed in KWT-BLA and used for the development of the correlations reported in the literature, which are obtained using smaller Re_p. Indeed, a linear trend can also be obtained from this work if $k_{eff,r}$ is determined for Re_p a ranging from 0 to 500. If h_w and $h_{w,ext}$ are compared, a significant difference up to 72% is identified, $h_{w,ext}$ being lower than h_w.

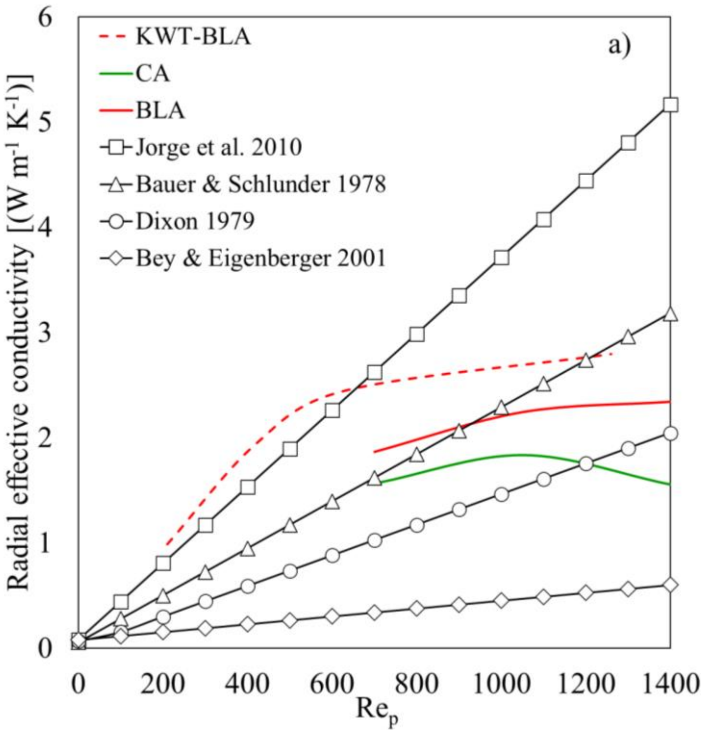

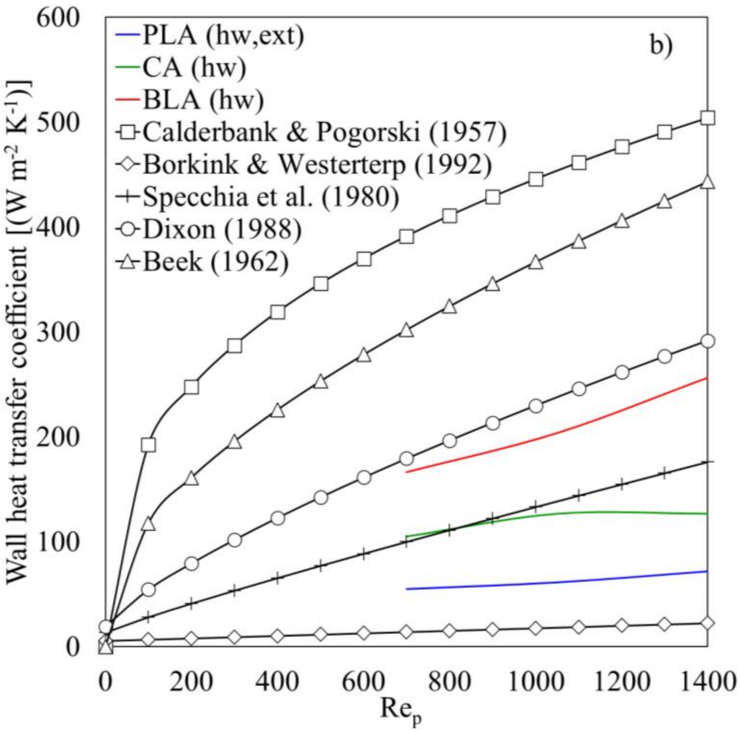

Figure 10. Heat transfer parameters estimated for the bench and industrial-scale packed bed and determined from correlations from the literature [15,46,101,107–112]. (a) radial effective conductivity and (b) the wall heat transfer coefficient

Table 4 . Heat transfer parameter estimates and their corresponding 95% confidence intervals for PLA (see Eq. (26)), CA and BLA (see Eq. S17 in Supporting information).

Case	**Re_p**	**$k_{eff,r}$**	**h_w or $h_{w,ext}$**
PLA[a]	700	-	55 ± 0.16
	1050	-	61 ± 0.30
	1400	-	71 ± 0.67
CA	700	1.56 ± 0.08	105 ± 0.98
	1050	1.83 ± 008	126 ± 1.03
	1400	1.55 ± 0.07	127 ± 0.97
BLA	700	1.86 ± 0.09	166 ± 1.42
	1050	2.24 ± 0.09	204 ± 1.51
	1400	2.34 ± 0.01	256 ± 1.56

$k_{eff,r}$ [=] W m^{-1} K^{-1}, h_w and $h_{w,ext}$ [=] W m^{-2} K^{-1}. [a] Pseudo-local $k_{eff,r,PL}(r)$ used in this case.

3.2.3 Radial heat transfer resistances analysis

With the heat transfer parameters estimated out of PLA, i.e., $h_{w,ext}$, and the pseudo-local $k_{eff,r,PL}(r)$, the internal and external heat transfer resistances and the U_w estimated from Eqs. (S24) – (S27) for the industrial-scale packed bed are calculated, see Table 5. Moreover, Figure 11 illustrates the variation of the heat transfer resistances for the industrial-scale packed bed.

Table 5. Internal and external heat transfer resistances.

Re_p	Internal Resistances [W^{-1} K]	External Resistances [W^{-1} K]	Internal resistances (%)	External resistances (%)	Estimated U_w [W m^{-2} K^{-1}]
700	0.00763	0.01822	29.58	70.42	75 ± 3.72
1050	0.00702	0.01634	30.07	69.93	81 ± 4.86
1400	0.00666	0.01400	32.29	67.71	78 ± 4.61

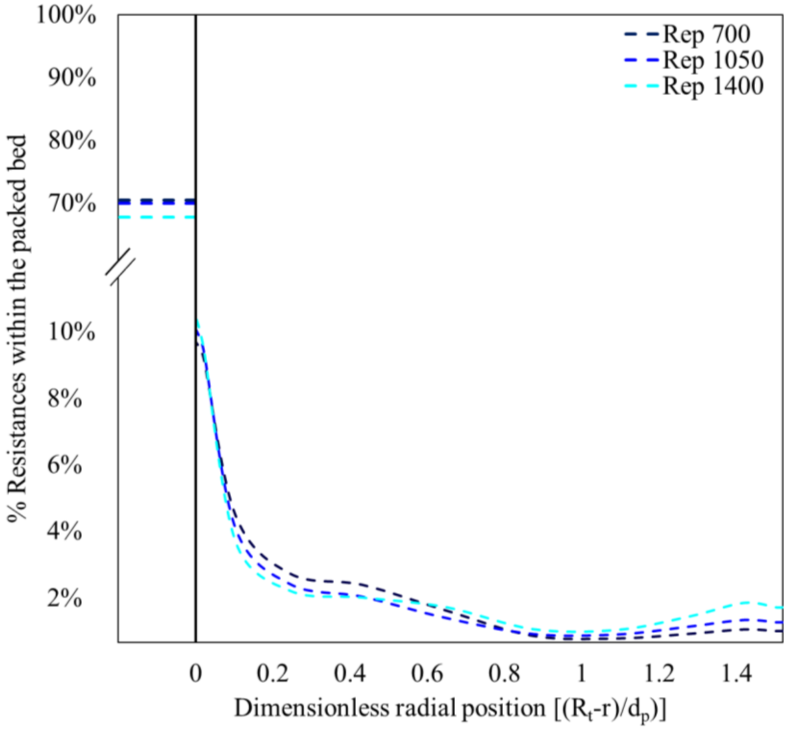

Figure 11. Percentage of external and internal heat transfer resistances within the industrial-scale packed bed at Re_p from 210 to 1400 Re_p.

The external and internal heat transfer resistances are ca. 70% and 30%, respectively.

However, heat transfer resistances are lower than 1% in most of the packed bed except in the wall zone. The heat transfer resistances, due to the $\delta_{HT,in}$ or shear stresses on the fluid by solid surfaces, start to have impact at ca. one pellet distance from the wall. Furthermore, between 0.7 pellets from the wall, the heat transfer resistances increase considerably from 1% up to 10%. This result is in line with the pseudo-local $k_{eff,r,PL}(r)$ variation showed in Figure 8. Additionally, the proper characterization of the pseudo-local $k_{eff,r,PL}(r)$ leads to a reliable heat transfer characterization of the heat pseudo-boundary layers inside and outside of the packed bed.

3.3 The Role of the PLA on the ODH-C_2 Industrial-Scale Reactor

With the aim of elucidating the importance of properly accounting for radial heat transfer and the uncertainties related to it when modeling an industrial reactor, the PLA is evaluated under reaction conditions for the ODH-C_2. Figure 12 illustrates the axial temperature profiles from the simulation results for the ODH-C_2 packed bed reactor at different bath temperatures. The results show a hot spot appearing at ca. 0.5 m from the reactor inlet for all the bath temperatures. However, as the bath temperature is increased, the hot spot is moved closer to the reactor inlet. Moreover, for the bath temperature of 480 °C, a hot spot temperature of ca. 820 °C is predicted (not shown in the figure). This runaway situation is in line with results reported in literature when an Eley-Rideal kinetic model is coupled with the BLA, i.e., a hot spot temperature of 717 °C[3] is predicted.

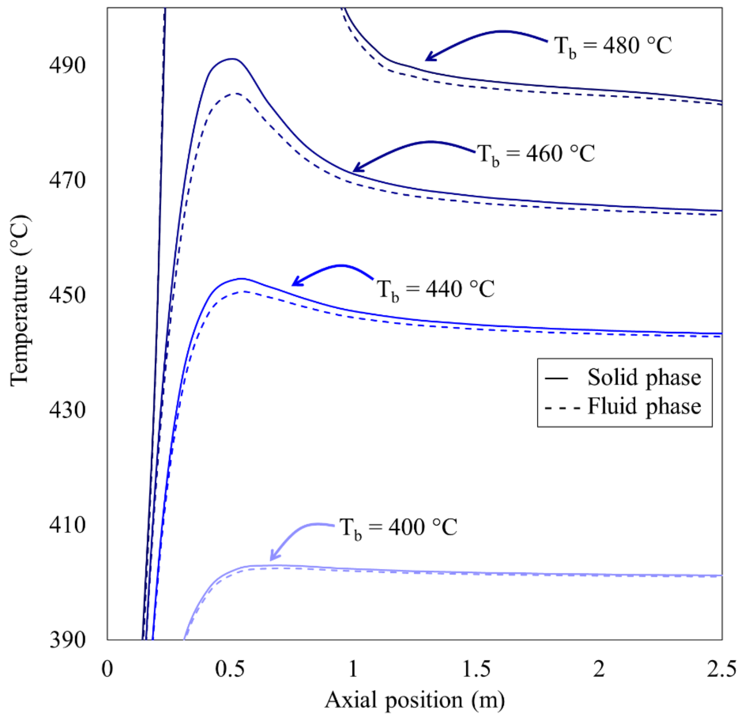

Figure 12. Axial temperature profiles predicted from PLA for the industrial-scale packed bed reactor at a Re_p of 1400 and inlet $C_2H_6/O_2/N_2$ = 9/7/84. The bath temperature ranges from 400 – 480 °C. Dashed lines describes fluid temperature and continuous lines the solid temperature.

Figure 13 shows the comparison between the axial temperature profiles within the packed bed reactor simulated by applying PLA and the conventional approaches CA and BLA at Re_p = 1400 and T_b = 440 °C. For the sake of brevity, the PLA, CA and BLA results related to the fractional coverage on the multi-metallic V-based catalyst, reaction rate profiles of CO_2 and the ethane conversion and ethylene yield along the packed bed reactor length are presented in Section F of the Supporting Information. The simulated axial temperature profile considering PLA is compared with those conventional approaches reported, i.e., CA and BLA, using both, the parameters estimated in this work and the ones reported in the literature for the ODH-C_2 [3]. It should be noted that the differences between the estimated values obtained here and those determined in literature for the classic approaches are due to the influence of the fluid dynamics as well as the regression method used. In this work, the fluid dynamic profile considers the mass conservation, and the parameters are estimated following a weighted regression method.

The simulations reported in the literature exhibit significant differences in simulated temperature profiles compared to the ones obtained with the PLA developed in this work. So far, there is a difference up to ca. 0.6 m and ca. 7 °C between the conventional approaches from literature and those reported in this work in the simulation of the hot spot position and magnitude, respectively, due to the difference of the heat transfer parameter values. When fluid dynamics is neglected, larger hot spot temperatures and larger displacements of the hot spot towards the reactor outlet are simulated. Moreover, fluid dynamics also impacts on the prediction of the broadness of the hot spot, i.e., the hot spot is wider when fluid dynamics is not accounted for. The inclusion of the velocity profile impacts on the convective transfer mechanisms, especially, at those zones of high void fraction, which in turn improves the heat transfer rates. These results show the sensitivity of the reaction kinetics to fluid dynamics and radial heat transfer impacting on both the microscopic and macroscopic performance of the of the reactor. Additionally, for all simulations, the temperature difference between the solid and fluid phase is the highest at the hot spot position, albeit that also there it remains below 5 °C.

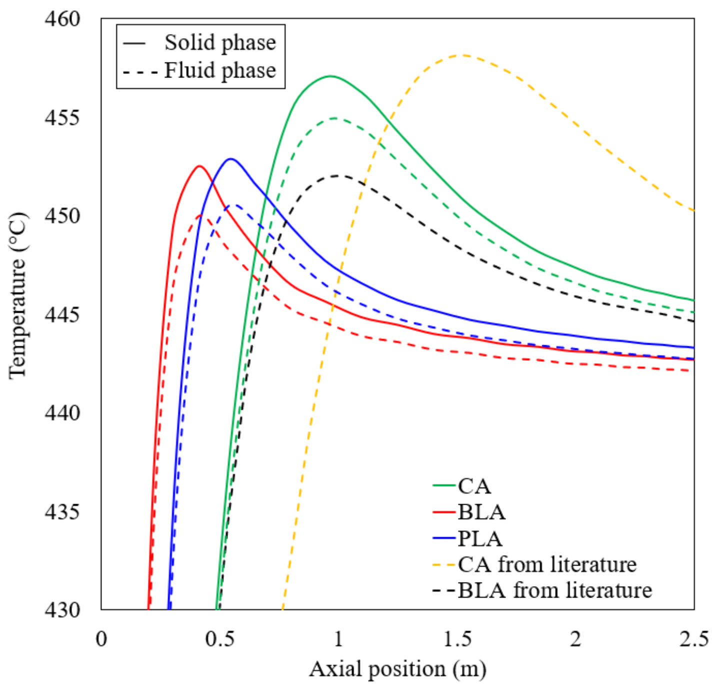

Figure 13. Axial temperature profiles predicted from PLA, CLA and BLA for the industrial-

scale packed bed reactor at a Rep of 1400, T_b = 440 °C and inlet $C_2H_6/O_2/N_2$ = 9/7/84. The parameters h_w [W m^{-2} K^{-1}] and $k_{eff,r}$ [W m^{-1} K^{-1}] from literature [3] are 91.5 and 1.17, respectively, for the CA, while for the BLA they are 155 and 1.65, respectively.

Using PLA a similar hot spot temperature is predicted as when using BLA. Using the former approach, the hot spot is simulated to occur at 0.52 m while with the latter it is simulated to occur already at 0.40 m from the reactor inlet. Similarities in the simulations can be related to the methodology implemented for the BLA, i.e., the initial guesses of h_w and $k_{eff,r}$ are obtained from the PLA and the final parameter values are determined via weighted regression. Moreover, heat transfer parameters are determined accounting for fluid dynamics such that they account for its impact on heat transfer once applied to the modeling of the industrial-scale reactor. PLA is developed accounting for capturing properly the heat transfer mechanisms inside the packed bed as well as the fluid dynamics effect on them. Moreover, $h_{w,ext}$ properly captures properly the external heat transfer mechanisms and it is estimated independently. To this end, future work must be aimed at validating the proposed heat transfer approach by predicting observations.

4. Conclusions

A newly developed methodology to reliably describe the performance a packed bed reactor with low tube to particle diameter ratio (d_t/d_p < 8 m_r m_s^{-1}) for highly exothermic reactions has demonstrated the need to account for both fluid dynamics and pseudo local radial effective thermal conductivity, $k_{eff,r,PLA}(r)$, including a reliable approximation to determine heat transfer resistances at the coolant side by estimating the external wall heat transfer coefficient, $h_{w,ext}$.

Firstly, the fluid dynamics within the packed bed was determined, using pressure drop experiments within a packed bed reactor, while ensuring the mass conservation criterion is met during the estimation of the effective viscosity, μ_{eff}. It was demonstrated that the velocity profiles, mainly in the wall zone, obtained from the non-conservative approaches overpredict the maximum velocity profile up to four times compared to the fluid dynamic model used in this work.

Secondly, the radial temperature predictions obtained via the PLA greatly improves the lack of temperature description along the radial axis, including the zone near to the wall using the conventional approaches. At ca. one-pellet distance from the wall the pseudo-local $k_{eff,r,PL}(r)$ has the highest value, because fluid velocity favors the dynamic heat transfer contribution. In the wall zone, $k_{eff,r,PL}(r)$ decreases as a result of the synergy between fluid dynamics and the heat boundary layers in the wall. Moreover, the pseudo-local parameters, i.e., $k_{1,h}$ and $k_{2,h}$, are in good agreement with those obtained at bench-scale and industrial-scale. This is mainly thanks to the operating conditions, the geometrical configuration and the packing that can be considered the same at both scales. Thus, an accurate scale-up can be ensured thanks to the use of the pseudo-local $k_{eff,r,PLA}(r)$ considering that the internal heat transfer mechanisms are very similar between both scales.

Then, proper characterization of the external heat transfer resistances encountered in the $\delta_{HT,ext}$ via the $h_{w,ext}$ demonstrated that the internal and external heat transfer resistances are ca. 30% and 70% of the total heat transfer resistances, respectively.

Ultimately, the PLA assessed on an industrial ODH-C_2 reactor predicted significant differences related to the hot spot within the packed bed reactor compared with CA, i.e., width of the hot spot and the position in the reactor where the hot spot is located. It should be noted that a reliable prediction of the hot spot is key to assess the reactor performance. On the other hand, PLA predictions versus BLA were similar, agreeing with the literature. The model developed in this work can be considered as one of the most consistent and generalized approximations to model heat transfer in the industrial-scale wall cooled packed bed reactor with a low tube-to-particle ratio. It overcomes historical limitations on the characterization of radial heat transfer, including the methodology applied to account for the effect of fluid dynamics on the PLA which properly captures the heat transfer mechanisms inside the packed bed reactor, mainly in those high void fraction zones. Moreover, PLA paves the way for suitable process concept design, optimization, and intensification in future works.

Declaration of Competing Interest

The authors declare that they have no known competing financial interests or personal relationships that could have appeared to influence the work reported in this paper.

Acknowledgments

Consejo Nacional de Ciencia y Tecnología (CONACyT) for providing a postgraduate fellowship. Division de Ciencias Básicas e Ingeniería from UAM-Iztapalapa for providing a special research fund for carrying out the investigation. Prof. H. F. López-Isunza for providing his heat transfer observations at the pilot-scale packed bed.

References

[1] A.I. Anastasov, A study of the influence of the operating parameters on the temperature of the hot spot in a fixed bed reactor, Chem. Eng. J. 86 (2002) 287–297. https://doi.org/10.1016/S1385-8947(01)00178-4.

[2] G.F. Froment, Fixed Bed Catalytic Reactor, Ind. Eng. Chem. 59 (1967) 18–27. https://doi.org/10.1007/978-3-662-44324-8_230.

[3] G. Che-Galicia, F. López-Isunza, E. Corona-Jiménez, C.O. Castillo-Araiza, The role of kinetics and heat transfer on the performance of an industrial wall-cooled packed-bed reactor: Oxidative dehydrogenation of ethane, AIChE J. 66 (2020). https://doi.org/10.1002/aic.16900.

[4] H. Delmas, G.F. Froment, A simulation model accounting for structural radial nonuniformities in fixed bed reactors, Chem. Eng. Sci. 43 (1988) 2281–2287. https://doi.org/10.1016/0009-2509(88)87116-1.

[5] C.O. Castillo-Araiza, F. López-Isunza, Modeling the partial oxidation of o-xylene in an

industrial packed-bed catalytic reactor: The role of hydrodynamics and catalyst activity in the heat transport, Ind. Eng. Chem. Res. 49 (2010) 6845–6853. https://doi.org/10.1021/ie901720z.

[6] C.O. Castillo-Araiza, F. López-Isunza, The role of catalyst activity on the steady state and transient behavior of an industrial-scale fixed bed catalytic reactor for the partial oxidation of o-xylene on V2O5/TiO2 catalysts, Chem. Eng. J. 176–177 (2011) 26–32. https://doi.org/10.1016/j.cej.2011.06.051.

[7] G.J.H. Tasker, The calculation of heat transfer and reaction rate in catalyst beds. Application of therory to phthalic anhydride pilot plant data, Inst. Chem. Eng. 24 (1946) 84–89.

[8] J.J. Lerou, G.F. Froment, Velocity, temperature and conversion profiles in fixed bed catalytic reactors, Chem. Eng. Sci. 32 (1977) 853–861. https://doi.org/10.1016/0009-2509(77)80071-7.

[9] T. Daszkowski, G. Eigenberger, A reevaluation of fluid flow, heat transfer and chemical reaction in catalyst filled tubes, Chem. Eng. Sci. 47 (1992) 2245–2250. https://doi.org/10.1016/0009-2509(92)87042-O.

[10] V. Blasco, C. Royo, A. Monzón, J. Santamaría, Catalyst sintering in fixed-bed reactors: Deactivation rate and thermal history, AIChE J. 38 (1992) 237–243. https://doi.org/10.1002/aic.690380209.

[11] Y.-S. Cheng, F. López-Isunza, T. Mongkhonsi, L. Kershenbaum, Estimation of catalyst activity profiles in fixed-bed reactors with decaying catalysts, Appl. Catal. A Gen. 106 (1993) 193–199. https://doi.org/10.1016/0926-860X(93)80177-R.

[12] J.N. Papageorgiou, G.F. Froment, Simulation models accounting for radial voidage profiles in fixed-bed reactors, Chem. Eng. Sci. 50 (1995) 3043–3056. https://doi.org/10.1016/0009-2509(95)00138-U.

[13] H.F. López-Isunza, Steady state and dynamic behaviour of an industrial scale fixed bed catalytic reactor, Ph. D. thesis, University of London, 1983.

[14] W.R. Paterson, J.J. Carberry, Fixed bed catalytic reactor modelling. The heat transfer problem, Chem. Eng. Sci. 38 (1983) 175–180. https://doi.org/10.1016/0009-2509(83)80149-3.

[15] O. Bey, G. Eigenberger, Gas flow and heat transfer through catalyst filled tubes, Int. J. Therm. Sci. 40 (2001) 152–164. https://doi.org/10.1016/S1290-0729(00)01204-7.

[16] D. Wen, Y. Ding, Heat transfer of gas flow through a packed bed, Chem. Eng. Sci. 61 (2006) 3532–3542. https://doi.org/10.1016/j.ces.2005.12.027.

[17] O.R. Derkx, A.G. Dixon, Effect of the wall Nusselt number on the simulation of catalytic fixed bed reactors, Catal. Today. 35 (1997) 435–442. https://doi.org/10.1016/S0920-5861(96)00210-6.

[18] J. Skrzypek, M. Grzesik, M. Galantowicz, J. Soliński, Kinetics of the catalytic air oxidation of o-xylene over a commercial V2O5-TiO2 catalyst, Chem. Eng. Sci. 40 (1985) 611–620. https://doi.org/10.1016/0009-2509(85)80005-1.

[19] C. McGreavy, E.A. Foumeny, K.H. Javed, Characterization of transport properties for fixed bed in terms of local bed structure and flow distribution, Chem. Eng. Sci. 41 (1986) 787–797. https://doi.org/10.1016/0009-2509(86)87159-7.

[20] P.H. Calderbank, K. Chandrasekharan, C. Fumagalli, The prediction of the performance of packed-bed catalytic reactors in the air-oxidation of o-xylene, Chem. Eng. Sci. 32 (1977) 1435–1443. https://doi.org/10.1016/0009-2509(77)80240-6.

[21] E. Tsotsas, E.U. Schlünder, Heat transfer in packed beds with fluid flow: remarks on the meaning and the calculation of a heat transfer coefficient at the wall, Chem. Eng. Sci. 45 (1990) 819–837. https://doi.org/10.1016/0009-2509(90)85005-X.

[22] I.M. Gerzeliev, A.M. Gyul’Maliev, A.Y. Popov, S.N. Khadzhiev, Thermodynamic and quantum-chemical study of the oxidative dehydrogenation of ethane to ethylene, Pet. Chem. 55 (2015) 146–153. https://doi.org/10.1134/S0965544115020097.

[23] M. Xie, H. Freund, Optimal reactor design and operation taking catalyst deactivation into account, Chem. Eng. Sci. 175 (2018) 405–415. https://doi.org/10.1016/j.ces.2017.10.010.

[24] A. Vandervoort, J. Thibault, Y.P. Gupta, Multi-Objective Optimization of an Ethylene Oxide Reactor, Int. J. Chem. React. Eng. 9 (2012). https://doi.org/10.1515/1542-6580.2548.

[25] Z. Till, T. Varga, J. Réti, T. Chován, Optimization Strategies in a Fixed-Bed Reactor for HCl Oxidation, Ind. Eng. Chem. Res. 56 (2017) 5352–5359.

https://doi.org/10.1021/acs.iecr.7b00750.

[26] Y. Nie, P.M. Witt, A. Agarwal, L.T. Biegler, Optimal active catalyst and inert distribution in catalytic packed bed reactors: Ortho-xylene oxidation, Ind. Eng. Chem. Res. 52 (2013) 15311–15320. https://doi.org/10.1021/ie4005699.

[27] O. Galan, V.G. Gomes, J. Romagnoli, K.F. Ngian, Selective oxidation of ethylene in an industrial packed-bed reactor: Modelling, analysis and optimization, Int. J. Chem. React. Eng. 7 (2009). https://doi.org/10.2202/1542-6580.2058.

[28] A.P. De Wasch, G.F. Froment, Heat transfer in packed beds, Chem. Eng. Sci. 27 (1972) 567–576. https://doi.org/10.1016/0009-2509(72)87012-X.

[29] S. Ströhle, A. Haselbacher, Z.R. Jovanovic, A. Steinfeld, Transient discrete-granule packed-bed reactor model for thermochemical energy storage, Chem. Eng. Sci. 117 (2014) 465–478. https://doi.org/10.1016/j.ces.2014.07.009.

[30] J. Votruba, V. Hlaváček, M. Marek, Packed bed axial thermal conductivity, Chem. Eng. Sci. 27 (1972) 1845–1851. https://doi.org/10.1016/0009-2509(72)85046-2.

[31] G. Che-Galicia, R.S. Ruiz-Martínez, F. López-Isunza, C.O. Castillo-Araiza, Modeling of oxidative dehydrogenation of ethane to ethylene on a MoVTeNbO/TiO2 catalyst in an industrial-scale packed bed catalytic reactor, Chem. Eng. J. 280 (2015) 682–694. https://doi.org/10.1016/j.cej.2015.05.128.

[32] A.I. Anastasov, An investigation of the kinetic parameters of the o-xylene oxidation process carried out in a fixed bed of high-productive vanadia-titania catalyst, Chem. Eng. Sci. 58 (2003) 89–98. https://doi.org/10.1016/S0009-2509(02)00431-1.

[33] G. Aparicio-Mauricio, R.S. Ruiz, F. López-Isunza, C.O. Castillo-Araiza, A simple approach to describe hydrodynamics and its effect on heat and mass transport in an industrial wall-cooled fixed bed catalytic reactor: ODH of ethane on a MoVNbTeO formulation, Chem. Eng. J. 321 (2017) 584–599. https://doi.org/10.1016/j.cej.2017.03.043.

[34] W. Kwapinski, Combined wall and thermal effects during non-isothermal packed bed adsorption, Chem. Eng. J. 152 (2009) 271–276. https://doi.org/10.1016/j.cej.2009.05.023.

[35] W. Kwapinski, M. Winterberg, E. Tsotsas, D. Mewes, Modeling of the Wall Effect in

Packed Bed Adsorption, Chem. Eng. Technol. 27 (2004) 1179–1186. https://doi.org/10.1002/ceat.200407001.

[36] C.O. Castillo-Araiza, H. Jiménez-Islas, F. López-Isunza, Heat-transfer studies in packed-bed catalytic reactors of low tube/particle diameter ratio, Ind. Eng. Chem. Res. 46 (2007) 7426–7435. https://doi.org/10.1021/ie070097z.

[37] A.I. Anastasov, The behaviour of a low-productive non-pretreated V2O5–TiO2 (anatase) catalyst for oxidation of o-xylene to phthalic anhydride, Chem. Eng. J. 109 (2005) 57–66. https://doi.org/10.1016/j.cej.2005.03.010.

[38] P.E.C. Burström, V. Frishfelds, A.L. Ljung, T.S. Lundström, B.D. Marjavaara, Modelling heat transfer during flow through a random packed bed of spheres, Heat Mass Transf. Und Stoffuebertragung. 54 (2018) 1225–1245. https://doi.org/10.1007/s00231-017-2192-3.

[39] E.M. Moghaddam, E.A. Foumeny, A.I. Stankiewicz, J.T. Padding, Heat transfer from wall to dense packing structures of spheres, cylinders and Raschig rings, Chem. Eng. J. 407 (2021) 127994. https://doi.org/10.1016/j.cej.2020.127994.

[40] E.M. Moghaddam, E.A. Foumeny, A.I. Stankiewicz, J.T. Padding, Fixed bed reactors of non-spherical pellets: Importance of heterogeneities and inadequacy of azimuthal averaging, Chem. Eng. Sci. X. 1 (2019) 100006. https://doi.org/10.1016/j.cesx.2019.100006.

[41] B. Hou, R. Ye, Y. Huang, X. Wang, T. Zhang, A CFD model for predicting the heat transfer in the industrial scale packed bed, Chinese J. Chem. Eng. 26 (2018) 228–237. https://doi.org/10.1016/j.cjche.2017.07.008.

[42] S. Wang, C. Xu, W. Liu, Z. Liu, Numerical study on heat transfer performance in packed bed, Energies. 12 (2019). https://doi.org/10.3390/en12030414.

[43] M. Behnam, A.G. Dixon, M. Nijemeisland, E.H. Stitt, A new approach to fixed bed radial heat transfer modeling using velocity fields from computational fluid dynamics simulations, Ind. Eng. Chem. Res. 52 (2013) 15244–15261. https://doi.org/10.1021/ie4000568.

[44] M. Fattahi, M. Kazemeini, F. Khorasheh, A. Darvishi, A.M. Rashidi, Fixed-bed multi-tubular reactors for oxidative dehydrogenation in ethylene process, Chem. Eng. Technol.

36 (2013) 1691–1700. https://doi.org/10.1002/ceat.201300148.

[45] V.A. Nikolov, A.I. Anastasov, Influence of the inlet temperature on the performance of a fixed-bed reactor for oxidation of o-xylene into phthalic anhydride, Chem. Eng. Sci. 47 (1992) 1291–1298. https://doi.org/10.1016/0009-2509(92)80249-C.

[46] L.M.D.M. Jorge, R.M.M. Jorge, R. Giudici, Experimental and numerical investigation of dynamic heat transfer parameters in packed bed, Heat Mass Transf. Und Stoffuebertragung. 46 (2010) 1355–1365. https://doi.org/10.1007/s00231-010-0659-6.

[47] M.L. Rodríguez, D.E. Ardissone, E. López, M.N. Pedernera, D.O. Borio, Reactor designs for ethylene production via ethane oxidative dehydrogenation: Comparison of performance, Ind. Eng. Chem. Res. 50 (2011) 2690–2697. https://doi.org/10.1021/ie100738q.

[48] A.I. Anastasov, A study of the influence of the operating parameters on the temperature of the hot spot in a fixed bed reactor, Chem. Eng. J. 86 (2002) 287–297. https://doi.org/10.1016/S1385-8947(01)00178-4.

[49] X. Guo, Y. Sun, R. Li, F. Yang, Experimental investigations on temperature variation and inhomogeneity in a packed bed CLC reactor of large particles and low aspect ratio, Chem. Eng. Sci. 107 (2014) 266–276. https://doi.org/10.1016/j.ces.2013.12.032.

[50] M. Giese, K. Rottschäfer, D. Vortmeyer, Measured and Modeled Superficial Flow Profiles in Packed Beds with Liquid Flow, AIChE J. 44 (1998) 484–490. https://doi.org/10.1002/aic.690440225.

[51] C.O. Castillo-araiza, F. Lopez-isunza, Hydrodynamic Models for Packed Beds with Low Tube-to-Particle Diameter Ratio Hydro, Int. J. Chem. React. Eng. 6 (2008) 1–14. https://doi.org/https://doi.org/10.2202/1542-6580.1550.

[52] G.A. Gómez-Ramos, C.O. Castillo-Araiza, S. Huerta-Ochoa, M. Couder-García, A. Prado-Barragán, Assessment of hydrodynamics in a novel bench-scale wall-cooled packed bioreactor under abiotic conditions, Chem. Eng. J. 375 (2019) 121945. https://doi.org/10.1016/j.cej.2019.121945.

[53] S. Ergun, Fluid flow through packed columns, Chem. Eng. Prog. 48 (1952) 89–94.

[54] S. Yagi, D. Kunii, N. Wakao, Studies on axial effective thermal conductivities in packed beds, AIChE J. 6 (1960) 543–546. https://doi.org/10.1002/aic.690060407.

[55] S. Yagi, N. Wakao, Heat and mass transfer from wall to fluid in packed beds, AIChE J. 5 (1959) 79–85. https://doi.org/10.1002/aic.690050118.

[56] T.H. Tsang, T.F. Edgar, J.O. Hougen, Estimation of heat transfer parameters in a packed bed, Chem. Eng. J. 11 (1976) 57–66. https://doi.org/10.1016/0300-9467(76)80006-8.

[57] S. Ströhle, A. Haselbacher, Z.R. Jovanovic, A. Steinfeld, The effect of the gas-solid contacting pattern in a high-temperature thermochemical energy storage on the performance of a concentrated solar power plant, Energy Environ. Sci. 9 (2016) 1375–1389. https://doi.org/10.1039/c5ee03204k.

[58] Z. Wan, J. Jiang, H. Ma, Y. Li, Y. Lu, F. Cao, A study of the heat transfer characteristics of novel Ni-foam structured catalysts, Can. J. Chem. Eng. 94 (2016) 2225–2234. https://doi.org/10.1002/cjce.22587.

[59] D.A. Asensio, M.T. Zambon, G.D. Mazza, G.F. Barreto, Heterogeneous two-region model for low-aspect-ratio fixed-bed catalytic reactors. Analysis of fluid-convective contributions, Ind. Eng. Chem. Res. 53 (2014) 3587–3605. https://doi.org/10.1021/ie403219q.

[60] S. Yagi, D. Kunii, Studies on heat transfer near wall surface in packed beds, AIChE J. 6 (1960) 97–104. https://doi.org/10.1002/aic.690060119.

[61] S. Yagi, D. Kunii, Studies on effective thermal conductivities in packed beds, AIChE J. 3 (1957) 373–381. https://doi.org/10.1002/aic.690030317.

[62] J.R. Fernández, J.M. Alarcón, J.C. Abanades, Investigation of a Fixed-Bed Reactor for the Calcination of CaCO3 by the Simultaneous Reduction of CuO with a Fuel Gas, Ind. Eng. Chem. Res. 55 (2016) 5128–5132. https://doi.org/10.1021/acs.iecr.5b04073.

[63] N. Wakao, S. Kaguei, T. Funazkri, Effect of fluid dispersion coefficients on particle-to-fluid heat transfer coefficients in packed beds. Correlation of nusselt numbers, Chem. Eng. Sci. 34 (1979) 325–336. https://doi.org/10.1016/0009-2509(79)85064-2.

[64] D.J. Gunn, M. Khalid, Thermal dispersion and wall heat transfer in packed beds, Chem. Eng. Sci. 30 (1975) 261–267. https://doi.org/10.1016/0009-2509(75)80014-5.

[65] M. Winterberg, E. Tsotsas, A. Krischke, D. Vortmeyer, A simple and coherent set of coefficients for modelling of heat and mass transport with and without chemical reaction in tubes filled with spheres, Chem. Eng. Sci. 55 (2000) 967–979.

https://doi.org/10.1016/S0009-2509(99)00379-6.

[66] E.A. Foumeny, J. Ma, Non-Darcian non-isothermal compressible flow and heat transfer in cylindrical packed beds, Chem. Eng. Technol. 17 (1994) 50–60. https://doi.org/10.1002/ceat.270170109.

[67] Linde Engineering, EDHOX(TM) technology, (n.d.). https://www.linde-engineering.com/en/process-plants/petrochemical-plants/edhox-technology/index.html?fbclid=IwAR0nPOmaju9OnUTgp0xKuTpdNzCTOghO0H_nYuFGL8xpTcchDmSJcQSVr-M (accessed June 28, 2022).

[68] K. Weissermel, H.-J. Arpe, Industrial Organic Chemistry, John Wiley & Sons, Weinheim, 2008.

[69] G. Che-Galicia, R. Quintana-Solórzano, R.S. Ruiz-Martínez, J.S. Valente, C.O. Castillo-Araiza, Kinetic modeling of the oxidative dehydrogenation of ethane to ethylene over a MoVTeNbO catalytic system, Chem. Eng. J. 252 (2014) 75–88. https://doi.org/10.1016/j.cej.2014.04.042.

[70] F.C. Blake, The Resistance of packing to fluid flow, Trans. Am. Inst. Chem. Eng. 14 (1922) 415–421.

[71] S.P. Burke, W.B. Plummer, Gas Flow through Packed Columns, Ind. Eng. Chem. 20 (1928) 1196–1200.

[72] A. Hernandez-Aguirre, E. Hernandez-Martinez, F. López-Isunza, C.O. Castillo, Framing a novel approach for pseudo continuous modeling using Direct Numerical Simulations (DNS): Fluid dynamics in a packed bed reactor, Chem. Eng. J. 429 (2022). https://doi.org/10.1016/j.cej.2021.132061.

[73] H. Darcy, Les Fontaines Publiques de la Ville de Dijon, Dalmon, Paris, 1856.

[74] P. Forchheimer, Tratado de Hidráulica, Ed. Labor, Barcelona, 1935.

[75] H.C. Brinkman, A calculation of the viscous force exerted by a flowing fluid on a dense swarm of particles, Flow, Turbul. Combust. 1 (1949) 27. https://doi.org/10.1007/BF02120313.

[76] A. De Klerk, Voidage variation in packed beds at small column to particle diameter ratio, AIChE J. 49 (2003) 2022–2029. https://doi.org/10.1002/aic.690490812.

[77] O. Bey, G. Eigenberger, Fluid flow through catalyst filled tubes, Chem. Eng. Sci. 52 (1997) 1365–1376. https://doi.org/10.1016/S0009-2509(96)00509-X.

[78] M. Winterberg, E. Tsotsas, Impact of tube-to-particle-diameter ratio on pressure drop in packed beds, AIChE J. 46 (2000) 1084–1088. https://doi.org/10.1002/aic.690460519.

[79] C.-H. Li, B.A. Finlayson, Heat Transfer in Packed Beds - A reevaluation, Chem. Eng. Sci. 32 (1977) 1055–1066.

[80] J. Marivoet, P. Teodoroiu, S.J. Wajc, Porosity, velocity and temperature profiles in cylindrical packed beds, Chem. Eng. Sci. 29 (1974) 1836–1840. https://doi.org/10.1016/0009-2509(74)87046-6.

[81] E.I. Smirnov, A. V. Muzykantov, V.A. Kuzmin, A.E. Kronberg, I.A. Zolotarskii, Radial heat transfer in packed beds of spheres, cylinders and Rashig rings Verification of model with a linear variation of λ_{er} in the vicinity of the wall, Chem. Eng. J. 91 (2003) 243–248. https://doi.org/10.1016/S1385-8947(02)00160-2.

[82] D. Vortmeyer, E. Haidegger, Discrimination of three approaches to evaluate heat fluxes for wall-cooled fixed bed chemical reactors, Chem. Eng. Sci. 46 (1991) 2651–2660. https://doi.org/10.1016/0009-2509(91)80058-7.

[83] G.F. Froment, Chemical Reactor Analysis and Design, 3rd Editio, John Wiley & Sons, New York, 2011.

[84] A. Stankiewicz, Advances in modelling and design of multitubular fixed- bed reactors, Chem. Eng. Technol. - CET. 12 (1989) 113–130. https://doi.org/10.1002/ceat.270120117.

[85] A. Jess, C. Kern, Modeling of Multi-Tubular Reactors for Fischer-Tropsch Synthesis, Chem. Eng. Technol. 32 (2009) 1164–1175. https://doi.org/10.1002/ceat.200900131.

[86] J. Chen, P. Bollini, V. Balakotaiah, Oxidative dehydrogenation of ethane over mixed metal oxide catalysts: Autothermal or cooled tubular reactor design?, AIChE J. 67 (2021). https://doi.org/10.1002/aic.17168.

[87] B.A. Finlayson, Nonlinear Analysis in Chemical Engineering, McGraw-Hill, New York, 2003.

[88] L. Lapidus, J.H. Seinfeld, Numerical solution of ordinary differential equations,

Academic Press, New York, 1971.

[89] P.T. Boggs, J.R. Donaldson, R.H. Byrd, R.B. Schnabel, ALGORITHM 676 ODRPACK : Software for Weighted Orthogonal Distance Regression, 15 (1989) 348–364. https://doi.org/10.1145/76909.76913.

[90] D.W. Marquardt, An algorithm for least-squares estimation of nonlinear parameters, J. Soc. Ind. Appl. Math. 11 (1963) 431–441. https://doi.org/https://doi.org/10.1137/0111030.

[91] C. Limberg, Computergenerierte Kugelschüttungen in zylindrischen Rohren als Basis für eine differenzierte Modellierung von Festbettreaktoren, Ph. D. thesis, Technischen Universität Cottbus, 2002.

[92] A.R. Morcom, Fluid Flow through granular materials, Trans. Inst. Chem. Eng. 24 (1946) 30–46.

[93] B. Eisfeld, K. Schnitzlein, The influence of confining walls on the pressure drop in packed beds, Chem. Eng. Sci. 56 (2001) 4321–4329. https://doi.org/10.1016/S0009-2509(00)00533-9.

[94] O. Bey, G. Eigenberger, Gas flow and heat transfer through catalyst filled tubes, Int. J. Therm. Sci. 40 (2001) 152–164. https://doi.org/10.1016/S1290-0729(00)01204-7.

[95] A.G. Dixon, D.L. Cresswell, Comments on “Estimation of heat transfer parameters in packed beds from radial temperature profiles” by J. J. Lerou and G. F. Froment, Chem. Eng. J. 17 (1979) 247–248. https://doi.org/10.1016/0300-9467(79)85020-0.

[96] M. Elsari, R. Hughes, Axial effective thermal conductivities of packed beds, Appl. Therm. Eng. 22 (2002) 1969–1980. https://doi.org/10.1016/S1359-4311(02)00117-5.

[97] T. Metzger, S. Didierjean, D. Maillet, Optimal experimental estimation of thermal dispersion coefficients in porous media, Int. J. Heat Mass Transf. 47 (2004) 3341–3353. https://doi.org/10.1016/j.ijheatmasstransfer.2004.02.024.

[98] G.F. Froment, Design of fixed-bed catalytic reactors based on effective transport models, Chem. Eng. Sci. 17 (1962) 849–859. https://doi.org/10.1016/0009-2509(62)87017-1.

[99] E.M. Moghaddam, E.A. Foumeny, A.I. Stankiewicz, J.T. Padding, Multiscale modelling of wall-to-bed heat transfer in fixed beds with non-spherical pellets: From particle-

resolved CFD to pseudo-homogenous models, Chem. Eng. Sci. 236 (2021) 116532. https://doi.org/10.1016/j.ces.2021.116532.

[100] A.G. Dixon, J.H. Van Dongeren, The influence of the tube and particle diameters at constant ratio on heat transfer in packed beds, Chem. Eng. Process. Process Intensif. 37 (1998) 23–32. https://doi.org/10.1016/S0255-2701(97)00033-0.

[101] J.G.H. Borkink, K.R. Westerterp, Influence of tube and particle diameter on heat transport in packed beds, AIChE J. 38 (1992) 703–715. https://doi.org/10.1002/aic.690380507.

[102] R.A. Dekhtyar’, D.P. Sikovsky, A. V. Gorine, V.A. Mukhin, Heat transfer in a packed bed at moderate values of the Reynolds number, High Temp. 40 (2002) 693–700. https://doi.org/10.1023/A:1020432619305.

[103] E.I. Smirnov, V.A. Kuzmin, I.A. Zolotarskii, Radial thermal conductivity in cylindrical beds packed by shaped particles, Chem. Eng. Res. Des. 82 (2004) 293–296. https://doi.org/10.1205/026387604772992891.

[104] J.C. Thoméo, J.T. Freire, Heat transfer in fixed bed: a model non-linearity approach, Chem. Eng. Sci. 55 (2000) 2329–2338. https://doi.org/10.1016/S0009-2509(99)00465-0.

[105] Y. Demirel, R.N. Sharma, H.H. Al-Ali, On the effective heat transfer parameters in a packed bed, Int. J. Heat Mass Transf. 43 (2000) 327–332. https://doi.org/10.1016/S0017-9310(99)00126-X.

[106] D.G. Bunnell, H.B. Irvin, R.W. Olson, J.M. Smith, Effective Thermal Conductivities in Gas-Solid Systems, Ind. Eng. Chem. 41 (1949) 1977–1981. https://doi.org/10.1021/ie50477a033.

[107] R. Bauer, E.U. Schlunder, Effective radial thermal conductivity of packings in gas flow, Int. Chem. Eng. 18 (1978) 189–204.

[108] A.G. Dixon, D.L. Cresswell, Theoretical prediction of effective heat transfer parameters in packed beds, AIChE J. 25 (1979) 663–676. https://doi.org/10.1002/aic.690250413.

[109] V. Specchia, G. Baldi, S. Sicardi, Heat transfer in packed bed reactors with one phase flow, Chem. Eng. Commun. 4 (1980) 361–380. https://doi.org/10.1080/00986448008935916.

[110] A.G. Dixon, Wall and particle-shape effects on heat transfer in packed beds, Chem. Eng. Commun. 71 (1988) 217–237. https://doi.org/10.1080/00986448808940426.

[111] J. Beek, Design of Packed Catalytic Reactors, Adv. Chem. Eng. 3 (1962) 203–271. https://doi.org/10.1016/S0065-2377(08)60060-5.

[112] P.H. Calderbank, L.A. Pogorski, Heat transfer in packed beds, Trans. Inst. Chem. Eng. 35 (1957) 195–207.